Heterotrimeric G-proteins in unfolded protein response mediate plant growth-defense tradeoffs upstream of steroid and immune signaling

Jimi C. Miller[*], Stacey A. Lawrence[†], Teresa Ceserani[†], Caroline L. Beakes[‡], Nicole K. Clay[†]

Current address:

[*]Department of Molecular Biophysics & Biochemistry, Yale University, New Haven, CT 06511

[†]Department of Molecular, Cellular & Developmental Biology, Yale University, New Haven, CT 06511

[‡]Department of Ecology & Evolutionary Biology, Yale University, New Haven, CT 06511

Author Contributions: C.B. contributed to characterization of *agg1 agg2/XVE:FLS2* lines. T.C. contributed to Endo H digestion. S.A.L. generated *agb1/35S:YFP-AGB1* lines, and contributed to qPCR of *ire1a/b*, Endo H digestion and MAPK activation of *agg1 agg2 atg7/3.* N.K.C. generated *XVE:BRI1-RFP* construct and *agg1 agg2/XVE:FLS2* lines, and contributed to Co-IPs and pathogen assays. J.C.M. generated all other constructs, and contributed to characterization of *agg1 agg2/XVE:FLS2* lines, Co-IPs and all other experiments. J.C.M. and N.K.C. interpreted the results and N.K.C. wrote the paper.

Abstract

Plants prioritize growth over defense to gain a competitive advantage for limited resources, but change priorities to successfully fight infection and herbivory. Despite the importance of growth-defense tradeoffs in optimizing plant productivity in natural and agricultural populations, the molecular mechanisms that link growth and immunity remain unclear. Here, we demonstrate that growth-defense tradeoffs between pathways activated by BRI1, a steroid receptor, and FLS2, an innate immune receptor, are uncoupled in an Arabidopsis mutant (*agg1 agg2*) lacking two redundant heterotrimeric G-protein gamma subunits that form stable heterodimers with the Gβ subunit AGB1 to control one arm of the unfolded protein response (UPR) independently of ER stress. Growth inhibition from induced immunity in wild-type plants is likely caused by AGB1-AGG1/2 dimers interacting with nascent BRI1 and FLS2 proteins on the endoplasmic reticulum (ER) membrane and repressing an UPR response that is hardwired to promote BRI1 protein biogenesis and FLS2 protein degradation via autophagy. The ability to unlock and fine-tune growth-defense tradeoffs through UPR signaling provides a novel strategy to increase the natural defenses of crops while maintaining optimal plant productivity.

Keywords: autophagy, anfolded protein response, heterotrimeric G-proteins, AGG1, AGB1, FLS2, BRI1, growth-defense tradeoffs

Significance Statement

Plants continually face a resource allocation dilemma – should they invest directly in growth to out-compete their neighbors for limited resources or invest directly in defense against herbivores and pathogens? Plants sense the competing demands of their surroundings through receptor proteins that are synthesized at high levels in ER. Here we show that plants use UPR to balance the synthesis of receptor proteins to favor defense over growth. This UPR response is mediated by heterotrimeric G-protein complexes whose signaling function in the ER is independent of their canonical functions at the plasma membrane. The uncoupling of growth and defense through UPR signaling provides a novel solution to the strong allocation tradeoffs against plant defensive traits as a consequence of plant domestication.

Introduction

Plants must maintain a precise balance between growth and defense in order to survive and reproduce, using a pool of limited resources (Huot et al. 2014). The tradeoff of shifting from growth to immunity upon detection of pathogens or herbivores has important ecological and agricultural consequences (Spoel and Dong, 2008; Dodds and Rathjen, 2010). The competing demands imposed on plants by their environments require mechanisms for sensing their surroundings and for effectively regulating the tradeoffs between growth and immunity. Over the past decade, a number of inhibitory crosstalks between individual pathways in growth and immunity have been characterized, including those involving the growth hormone brassinosteroids (BR)-perceiving transmembrane leucine-rich repeat-receptor kinase (LRR-RK) Brassinosteroid-Insensitive-1 (BRI1), bacterial flagellin-recognizing transmembrane LRR-RK Flagellin-Sensing-2 (FLS2), defense hormone salicylic acid (SA), and unfolded protein response (UPR) (Li and Chory, 1997; Gómez-Gómez and Boller, 2000; Rivas-San Vicente and Plasencia, 2011; Albrecht et al., 2012; Belkhadir et al., 2012; Nagashima et al., 2014; Jiménez-Góngora et al., 2015). The shared signaling components between BRI1- and FLS2-mediated signaling and between SA and UPR signaling have been characterized to mediate not only signal crosstalk between these pathways but also tradeoffs between growth and defense (Lozano-Durán et al., 2013; Fan et al., 2014; Meng et al., 2017).

The ER is the production and folding compartment for membrane proteins of the cell. Quality control mechanisms in the ER ensure that only properly folded proteins exit the ER via the secretory pathway, while improperly folded proteins exit the ER through ER-associated degradation (ERAD) or autophagy (Smith et al., 2011; Pu and Bassham, 2013). UPR is an evolutionarily conserved adaptive response triggered by the accumulation of unfolded proteins in the ER and aimed at restoring protein-folding homeostasis. However, the main function of UPR in vertebrates and plants is in growth and defense, where it acts as an anticipatory response that is activated well before the disruption of protein homeostasis and aimed at

handling high folding loads that are part of normal physiology (Janssens et al., 2014; Bao and Howell, 2017). The UPR signaling pathway in Arabidopsis has three overlapping but independent arms (Ruberti and Brandizzi, 2014). One arm is mediated by two homologs of the evolutionarily conserved transmembrane ER kinase/RNA splicing factor IRE1 (IRE1A and IRE1B), whose primary target is the transcription factor *bZIP60* mRNA (Koizumi et al., 2001; Deng et al., 2011). The second arm is mediated by ER membrane-associated transcription factors bZIP17 and bZIP28, which are functional homologs of ATF6 in metazoans (Liu et al., 2007). The last arm is mediated by the ER membrane-localized heterotrimeric G-protein β subunit AGB1 (Wang et al., 2007; Chen and Brandizzi, 2012) and possibly by other G-protein subunits, such as Gα subunits XLG1/2/3 and the Gγ subunits AGG1/2/3 (Chakravorty et al., 2015). AGB1 is required for UPR signaling under ER stress conditions (Wang et al., 2007; Chen and Brandizzi, 2012), but its UPR function in growth and defense has not yet been reported.

Heterotrimeric G-proteins are the most commonly used signal transducers in eukaryotic cells. They transduce signals at the cytosolic surfaces of the plasma membrane (PM) and endoplasmic reticulum (ER) as Gαβγ heterotrimers, Gβγ heterodimers or individual Gα subunits (Weiss et al., 1997; Kaydamov et al., 2000; Wang et al., 2007; Hewavitharana and Wedegaertner, 2012; Giannotta et al., 2012; Klayman and Wedegaertner, 2017). Gβγ dimers and Gαβγ trimers are thought to assemble on the ER membrane (Dupre et al., 2007; Marrari et al., 2007), and are anchored to membranes by virtue of lipid modifications on the Gα and Gγ subunits (Wedegaertner 1998; Adjobo-Hermans et al., 2006; Zeng et al., 2007). Arabidopsis has at least four Gα (GPA1, XLG1/2/3), a Gβ (AGB1), and three Gγ (AGG1/2/3) subunits (Chakravorty et al., 2015; Maruta et al., 2015; Thung et al., 2012), and likely more non-canonical G-protein subunits yet to be discovered (Lee and Assmann, 1999; Chakravorty et al., 2011). All known G-protein subunits are involved in some aspect of growth and development (Lease et al., 2001; Ullah et al., 2001; Ullah et al., 2003; Trusov et al., 2007; Ding et al., 2008; Chakravorty et al., 2011). In addition, a subset – Gα GPA1, Gβ AGB1 and Gγ AGG3 – are

involved in BR signaling in sugar-responsive growth (Peng et al., 2018), and all save two – XLG1 and AGG3 – are involved in flagellin signaling (Ishikawa 2009; Zhang et al., 2008; Zhu et al., 2009; Liu et al., 2013; Torres et al., 2013; Maruta et al., 2015; Miller et al., 2016). Recently, AGB1 has been shown to be a shared component in BR and flagellin signaling via interactions with corresponding receptors BRI1 and FLS2, presumably at the PM, and with the BR transcription factor BES1 in the nucleus, downstream of receptor signaling (Liang et al., 2016; Peng et al., 2018; Zhang et al., 2018). The essential role of G-proteins in both BR and flagellin signaling pathways suggests that they may function as rate-limiting factors between both pathways to mediate tradeoffs between growth and immunity.

Here, we show that AGB1 and Gγ subunits AGG1 and AGG2 work together in UPR signaling to mediate growth-defense tradeoffs that are upstream of BR and flagellin signaling and independent of ER stress. Specifically, they interact with nascent FLS2 and BRI1 proteins at the ER membrane and repress an UPR response that is hardwired to promote BRI1 protein biogenesis and FLS2 protein degradation via autophagy.

Results

Increased BRI1 signaling likely contributes to enhanced growth of *agg1 agg2*. While the loss-of-function *agb1* mutant exhibited growth defects due to its involvement in multiple hormone signaling pathways, (Ullah et al., 2003; Chen et al., 2004; Pandey et al., 2006; Trusov et al., 2006), the loss-of-function *agg1 agg2* double mutant exhibited increased vegetative growth and faster transition to inflorescence development compared to WT and *agb1* (**Fig. 1A;** *SI Appendix*, Fig. S1*A*). To identify the Gγ subunit(s) interacting with AGB1 in the crosstalk between BR and flagellin signaling, we performed a time course of seedling growth and BRI1 protein expression under normal growth conditions. The loss-of-function *agg1 agg2* mutant exhibited increased BRI1 protein expression relative to WT after day 6 post-germination, correlating with its increased growth after day 8 (**Fig. 1B–D**; *SI Appendix*, Fig. S2*A*). Although the loss-of-function *agb1* mutant exhibited normal seedling growth (**Fig. 1C**), it displayed slightly increased BRI1 protein expression after day 6 (**Fig. 1C–D**). To confirm our genetic results, we used the estrogen receptor-based *XVE* system to drive *AGG1-RFP* expression in *agg1 agg2* (*agg1 agg2/XVE:AGG1-RFP*). Induced expression of *AGG1-RFP* reduced BRI1 protein expression to WT level or below in 9-day-old seedlings (**Fig. 1D**).

To investigate whether increased BRI1 protein expression in *agg1 agg2* and *agb1* is due to increased transcription and/or translation, we measured *BRI1* gene expression during a 24-hr time period in 4-hr increments and measured BRI1 protein expression in 5.5-day-old seedlings pretreated with the protein translation inhibitor cycloheximide (CHX). *agg1 agg2* and *agb1* plants exhibited increased *BRI1* expression relative to WT throughout the time period (*SI Appendix*, Fig. S2*B*), consistent with the observed BRI1 protein expression pattern (**Fig. 1D**) and indicative of G-protein-dependent transcription. In addition, CHX treatment inhibited developmental upregulation of BRI1 protein expression in *agg1 agg2* and *agb1* (**Fig. 1E**). These results indicate that increased transcription and translation are likely responsible for the increased BRI1 protein expression in G-protein mutants. *BRI1*-overexpression has been

demonstrated to confer enhanced BR signaling in plants (Belkhadir et al., 2012), whereas mutants impaired in BRI1 signal transduction, such as *bak1,* exhibited reduced growth (**Fig. 1C**; Clouse et al., 1996; Li et al., 2002). Our findings suggest that BR signal transduction is increased in the *agg1 agg2* mutant, contributing to its increased growth under normal growth conditions.

Increased FLS2 protein turnover contributes to enhanced growth of *agg1 agg2* under defense-inducing conditions. *BRI1*-overexpression also confers reduced FLS2-mediated immune responses (Belkhadir et al., 2012). To investigate whether transient growth-defense tradeoffs are affected in the *agg1 agg2* mutant upon flagellin perception, we measured seedling growth inhibition (SGI) in response to the active epitope of bacterial flagellin, flg22. Consistent with *BRI1*-overexpression plants (Belkhadir et al., 2012), *agg1 agg2* exhibited a reduced flg22-induced growth inhibition response relative to WT after day 5 (**Fig. 2A**; *SI Appendix*, Fig. S3*A–B*), whereas induced expression of *AGG1-RFP* restored flg22-induced growth inhibition in *agg1 agg2* to WT level (**Fig. 2A**). Although *agb1* exhibited a normal growth inhibition response (**Fig. 2A**), we used the *35S* system to drive *YFP-AGB1* expression in *agb1* (*agb1/35S:YFP-AGB1*). Constitutive expression of *YFP-AGB1* increased flg22-induced growth inhibition in *agb1* relative to WT (**Fig. 2A**). As a control, we measured FLS2 protein expression in *agg1 agg2* and *agb1* and found that they exhibited reduced FLS2 protein expression (**Fig. 2B**), whereas induced expression of *AGG1-RFP* restored FLS2 protein expression to or above that of WT (**Fig. 2B**). To confirm these results, we measured FLS2 protein expression during a 24-hr time period in 4-hr increments. *agg1 agg2* exhibited decreased FLS2 protein expression relative to WT throughout most of the day with peak reductions occurring at night (**Fig. S2C**). To investigate whether reduced FLS2 protein expression in *agg1 agg2* is due to transcription, translation and/or protein degradation, we measured *FLS2* gene expression during a 20-hr period in non-treated plants and measured FLS2 protein expression during a 16-hr period in plants pretreated with CHX. *agg1 agg2* and *agb1* exhibited increased *FLS2* expression relative to WT 4 hr after

dawn and reduced *FLS2* expression 4 hr after dusk, which does not correlate with the observed FLS2 protein expression pattern (*SI Appendix*, Fig. S3*C–D*) and is indicative of G-protein-dependent transcription. In addition, CHX treatment revealed that FLS2 protein expression was more reduced in *agg1 agg2* relative to WT at an earlier time point (**Fig. 2D**), indicative of increased protein degradation. These findings suggest that increased FLS2 protein turnover contributes to the enhanced growth observed in *agg1 agg2* under defense conditions.

To determine whether the increased turnover in *agg1 agg2* affects newly synthesized FLS2 proteins on the ER membrane or mature FLS2 proteins on the PM, we performed aqueous two-phase partitioning of total membrane proteins and measured FLS2 abundance among microsomal membrane (MM) and PM proteins. *agg1 agg2* exhibited a decrease in FLS2 protein expression at both membrane populations (*SI Appendix*, Fig. S3*E*). Since membrane proteins on the PM must exit the ER, this result suggests that nascent FLS2 proteins at the ER membrane are targeted for turnover in the *agg1 agg2* mutant.

To confirm that increased BRI1 signaling and/or increased FLS2 turnover in *agg1 agg2* contributes to reduced FLS2-mediated immune responses, we measured activation of mitogen-associated kinases (MAPKs) and callose deposition at the cell wall in response to flg22. *agg1 agg2* exhibited reduced flg22-induced MAPK activation and callose deposition responses relative to WT (*SI Appendix*, Figs. S4 and S5)**,** whereas induced expression of *AGG1-RFP* restored MAPK activation in *agg1 agg2* to WT level (*SI Appendix*, Fig. S4*C*) and increased callose deposition 2-fold (*SI Appendix*, Fig. S5). On the other hand, *agb1* exhibited a normal flg22-induced MAPK activation response (*SI Appendix*, Fig. S4*A*). *agb1* also exhibited a reduced callose deposition response that could not be rescued by constitutive expression of *AGB1* (*SI Appendix*, Fig. S5), likely due to poor *35S* promoter expression in seedling leaves (Kamo et al., 2000).

Growth and defense are uncoupled in *agg1 agg2* mutant. BR signaling has been shown to antagonize FLS2-mediated immune responses downstream of receptor signaling (Albrecht et

al., 2012; Belkhadir et al., 2012; Lozano-Durán et al., 2013; Fan et al., 2014). *agg1 agg2* exhibits enhanced growth under growth-inducing conditions and defense-inducing conditions, consistent with the increased and decreased expression of respective BRI1 and FLS2 in this mutant (**Figs. 1 and 2**). To investigate whether the negative crosstalk between BR and flagellin signaling is preserved in *agg1 agg2*, we measured three FLS2-mediated immune responses (i.e., defense response gene transcription, callose deposition and seedling growth inhibition) in response to the BR hormone 24-epibrassinolide (BL). Consistent with a previous report (Albrecht et al., 2012), MAPK-activated transcription of defense response genes *CYP81F2* and *CYP82C2* (Boudsocq et al., 2010) was reduced in WT seedlings in response to co-treatment with 1 µM BL and 100 nM flg22 compared to flg22 treatment alone (**Fig. 3A**). Similarly, callose deposition and growth inhibition were reduced in WT plants and unchanged in BRI1 signaling mutant *bak1* in response to co-treatment with BL and flg22 (**Fig. 3B–C**). By contrast, *agg1 agg2* exhibited no changes in defense gene transcription, smaller reductions in callose deposition relative to WT, and no changes in growth inhibition in response to BL and flg22 (**Fig. 3A–C**), whereas *agb1* resembled WT plants in all three FLS2-mediated immune response (**Fig. 3A–C**). These results indicate that growth and defense are uncoupled in the *agg1 agg2* mutant.

Interestingly, *agg1 agg2* and *agb1* exhibited reduced growth in response to 1 µM BL alone (**Fig. 3C**). High BR concentrations and/or signaling can inhibit growth (Clouse et al., 1996; Müssig et al., 2003; González-García et al., 2011), indicating that an appropriate intensity of BR signaling is important for optimal plant growth. To investigate whether increased BRI1 signaling in *agg1 agg2* is responsible for its increased insensitivity to exogenous BL application, we measured hypocotyl lengths in response to 1 and 10 µM BL. At 1 µM BL, the concentration reported to result in nearly full BL responsiveness in this tissue (Clouse et al., 1996), *agg1 agg2* and *agb1* exhibited a normal hypocotyl elongation response, whereas at 10 µM BL, they exhibited reduced BL responsiveness (*SI Appendix*, Fig. S6*A–B*). By contrast, induced expression of *AGG1-RFP* and constitutive expression of *YFP-AGB1* restored WT level of BL

sensitivity in respective *agg1 agg2* and *agb1* plants treated with 10 µM BL (*SI Appendix*, Fig. S6*B*). These results lend further support to increased BRI signaling occurring in G-protein mutants.

AGG1 and AGG2 are involved in UPR signaling in the absence of ER stress. AGB1 is enriched in the ER, where it functions as an UPR sensor during ER stress (Wang et al., 2007; Chen and Brandizzi, 2012). To investigate whether UPR signaling is affected in the *agg1 agg2* mutant, we measured seedling growth inhibition in response to ER stress induced by tunicamycin (Tn). Consistent with previous reports on the *agb1* mutant (Chen and Brandizzi, 2012; Chakravorty et al 2015), *agg1 agg2* is hyper-responsive to long-term (14 days) Tn-induced ER stress (**Fig. 4A**). In fact, dose-response curves indicate that *agg1 agg2* is more sensitive to Tn-induced ER stress than UPR signaling mutants *agb1* and *ire1a ire1b* (**Fig. 4A**). We then looked for changes in expression of UPR-activated genes in response to short-term (5 hr) Tn-induced ER stress and observed increased expression of *IRE1A* and *IRE1B*, their spliced target *bZIP60s*, and G-protein genes *AGB1, AGG1* and *AGG2* (**Fig. 4B**). Furthermore, *IRE1A, IRE1B* and *bZIP60s* were expressed normally in *agg1 agg2* and *agb1* mutants in response to short-term Tn-induced ER stress, whereas *AGG1* and *AGB1* were downregulated in *ire1a ire1b* mutant (**Fig. 4B**), indicative of IRE1A/B-dependent transcription.

IRE1A/B and AGB1 have been shown to respectively upregulate and downregulate the gene expression of the chaperone and IRE1A/B ligand BIP3 in response to long-term (3 days) Tn-induced ER stress (Chen and Brandizzi, 2012). Consistent with this finding, combined BIP1–3 (BIP) protein expression was reduced in *ire1a ire1b* relative to WT and *agb1* independent of ER stress, whereas ER stress-induced expression of folding catalyst PDI was unchanged in *agg1 agg2, agb1* and *ire1a ire1b* (*SI Appendix*, Fig. S7). Furthermore, *agg1 agg2* exhibited increased *BIP3* expression in response to short-term (5 hr) Tn-induced ER stress (**Fig. 4B**), whereas *BIP3* expression was unchanged in WT, *ire1a ire1b,* and *agb1* (**Fig. 4B**). More importantly, *ire1a ire1b* exhibited normal BRI1 and FLS2 protein expression (**Figs. 1C and 2B**),

and *agg1 agg2* and *agb1* exhibited no upregulation of *IRE1A/B, BIP3* and *bZIP60s* gene expression or PDI protein expression in the absence of ER stress (**Fig. 4B;** *SI Appendix*, Fig. S7). Thus, IRE1A/B and G-proteins have distinct UPR functions independent of ER stress. Altogether, these findings suggest that AGB1 and AGG1/2 work together to promote FLS2 biogenesis and repress BRI1 biogenesis through UPR signaling in the absence of ER stress.

AGB1-AGG1/2 interact with FLS2 and BRI1 at the ER membrane. AGB1 forms obligate heterodimers with AGG1 and AGG2 (Mason and Botella, 2000; Adjobo-Hermans et al., 2006; Chakravorty and Botella, 2007), and interacts with FLS2 and BRI1 *in vivo* (Liang et al., 2016; Peng et al., 2018). To investigate whether AGB1 and/or AGG1 interact with nascent FLS2 and BRI1 proteins at the ER membrane, we first detected AGG1, AGB1, BRI1 and FLS2 proteins that were C-terminally tagged with GFP or RFP in *Nicotiana benthamiana* leaves. Consistent with a previous report (Adjobo-Hermans et al., 2006), AGG1 co-localized with AGB1 at the PM (*SI Appendix*, Fig. S8*A*), and with FLS2 at plasmolysis-induced Hechtian strands, which are PM fragments still attached to the cell wall and separated from the cytosol (*SI Appendix*, Fig. S8*B*). AGG1 also co-localized with AGB1 and FLS2 at the highly reticulated ER membrane and with the ER protein marker HDEL (**Fig. 4A**; Gomord et al., 1997). The ER localization of AGG1 was further validated in *agg1 agg2/XVE:AGG1-RFP* plants (*SI Appendix*, Fig. S8*C*). AGG1 and AGB1 also co-localized with BRI1 at the ER membrane (*SI Appendix*, Fig. S8*D*). These results confirmed that the C-terminal tag did not disrupt AGG1's lipid modification and subsequent localization of AGG1 and its partner AGB1 to membranes.

We then immunoprecipitated AGG1-GFP and AGB1-GFP proteins from PM and MM protein extracts of *N. benthamiana* leaves as well as YFP-AGB1 and AGG1-RFP proteins from PM and MM protein extracts of Arabidopsis seedlings. FLS2-RFP and native FLS2 protein co-immunoprecipitated with respective AGG1-GFP and AGG1-RFP at the PM and MM (**Fig. 4B–C**). Native FLS2 also co-immunoprecipitated with YFP-AGB1 at the PM and MM in Arabidopsis (**Fig. 4C**). Similarly, BRI1-RFP co-immunoprecipitated with AGG1-GFP and AGB1-GFP at the

PM and MM in *N. benthamiana* (*SI Appendix*, Fig. S9). We were unable to confirm the BRI1-AGB1/AGG1 interactions in Arabidopsis due to the relatively weak antibody for the native BRI1 protein. Our findings suggest that AGG1 and AGB1 work together in UPR signaling to mediate growth-defense tradeoffs that involve direct interactions with nascent FLS2 and BRI1 proteins at the ER membrane.

Combination of *agg1 agg2* and *atg7/3* promotes robust growth and defense. To investigate whether FLS2 protein is being targeted by UPR-associated protein degradation processes in *agg1 agg2,* we measured FLS2 protein expression in seedlings pretreated with chemical inhibitors of ERAD and autophagy. Co-treatment of proteasome inhibitor MG132 and autophagy inhibitor E-64D (Oh-ye et al., 2011) or concanamycin A (Con A) (Yoshimoto et al., 2004), or that of E-64d and Con A restored FLS2 protein expression in *agg1 agg2* to or above WT level, whereas single treatments did not (*SI Appendix*, Fig. S10*A*). We then measured the flg22-induced seedling growth inhibition response in the presence of these inhibitors. Co-treatment of MG132 and E-64d restored growth inhibition in *agg1 agg2* to WT level, whereas single treatments did not (*SI Appendix*, Fig. S10*B*). Furthermore, MG132 and E-64d co-treatments did not significantly affect growth in WT or *agg1 agg2* plants relative to mock treatment (*SI Appendix*, Fig. S10*C*), whereas treatments with Con A at nano-molar concentrations proved toxic and were thus removed from analysis. These data suggest that UPR-associated degradation of nascent FLS2 proteins involves autophagy and/or ERAD.

To confirm these findings, we knocked out the two autophagy-requiring ubiquitin-like conjugation systems in the *agg1 agg2* mutant by introducing loss-of-function mutations in the E1-like *ATG7* and E2-like *ATG3* genes by intermutant crosses (Klionsky 2005; Ohsumi 2001; Kim et al., 2012). We then measured flg22-induced growth inhibition and FLS2 protein expression in the *agg1 agg2 atg7* and *agg1 agg2 atg3* triple mutants. Flg22-induced growth inhibition and FLS2 protein expression were both restored in *agg1 agg2 atg7* and *agg1 agg2 atg3* to or greater than WT levels (**Fig. 6A–B**). To confirm that the recovered FLS2 proteins

were not retained in the ER, we digested the proteins with endoglycosidase H (Endo H) enzyme to cleave off their ER-specific glycans. FLS2 proteins that exit the ER will acquire Golgi-specific glycans that are resistant to Endo H digestion. Wild-type FLS2 proteins were partially deglycosylated upon Endo H digestion, whereas FLS2 proteins produced in the *mns1 mns2 mns3* mutant lacked Golgi-specific glycans (Liebminger et al., 2009), and thus were fully deglycosylated (*SI Appendix*, Fig. S11*A*). FLS2 proteins in the *agg1 agg2 atg7* and *agg1 agg2 atg3* plants were partially deglycosylated (*SI Appendix*, Fig. S11*A*), indicating that they have exited the ER *en route* to the PM.

We then investigated whether inhibition of autophagy is sufficient to restore growth-defense tradeoffs in the *agg1 agg2* mutant. *agg1 agg2* exhibited reduced seedling flg22-induced MAPK activation response and adult leaf resistance to the virulent bacterial pathogen *Pseudomonas syringae* pv. *tomato* DC3000 (*Pto* DC3000), as well as enhanced seedling, vegetative and reproductive growth relative to WT (**Fig. 6D**; *SI Appendix*, Figs. S1B and S11*B*). By contrast, *agg1 agg2 atg7* and *agg1 agg2 atg3* exhibited normal flg22-induced MAPK activation response and anti-bacterial defense, as well as normal growth and development relative to WT and *atg7/3* single mutants (**Fig. 6C-D**; *SI Appendix*, Figs. S1 and S11*B*). Furthermore, *agb1* exhibited reduced anti-bacterial defense, whereas the double mutants *agb1 atg7* and *agb1 atg3* exhibited normal bacterial resistance and adult development relative to WT and *atg7/3* single mutants (*SI Appendix*, Figs. S1 and S12). These findings indicate that AGB1 and AGG1/2 work together in UPR signaling to mediate growth-defense tradeoffs that involve repression of FLS2 protein degradation by autophagy.

UPR is hardwired to promote FLS2 protein degradation in the absence of ER stress. To investigate whether UPR in growth-inducing conditions requires protein 'triggers' for selective protein degradation, we used the *XVE* system to drive expression of a *FLS2* transgene in *agg1 agg2* (*agg1 agg2/XVE:FLS2*). To our surprise, we obtained three independent lines (#2–4), whose FLS2 protein expression was knocked-down to undetectable levels with or without *FLS2*

induction, whereas their seedling growths were unchanged upon *FLS2* induction (**Fig. 7A**; *SI Appendix*, Fig. S13). We also obtained one line (#1) whose FLS2 protein expression and growth were increased to and greater than WT levels, respectively, in the absence of *FLS2* induction (**Fig. 7A**; *SI Appendix*, Fig. S13). This finding lends further support to the uncoupling of growth and defense in the *agg1 agg2* mutant. Leaky expression of the *XVE* system has been reported in rice (Okuzaki et al., 2011) and appears to be sufficient to activate further increases in FLS2 production and/or degradation. To confirm that FLS2 production and subsequent degradation were activated in *agg1 agg2/XVE:FLS2* lines #2–4, we measured their FLS2 protein expression after gene induction and co-treatment with E-64d and Con A and found FLS2 protein expression to be restored to WT level for all three lines (**Fig. 7B**). Taken together, these data suggest that in the absence of AGG1/2 and ER stress, UPR is hardwired to promote BRI1 protein biogenesis and FLS2 protein degradation via autophagy while at the same time responsive to transient and minute increases in FLS2 protein expression (**Fig. 7C**).

Discussion

A key innovation of our study was the development of the *agg1 agg2 atg7/3* mutants and the *agg1 agg2/XVE:FLS2* transgenic lines. The removal of functionally redundant Gγ subunits caused hyperactivation of BRI1 protein biogenesis and FLS2 protein degradation and the uncoupling of growth and defense, while the removal of autophagy restored FLS2-mediated immune responses in *agg1 agg2* mutant. As a consequence, even though *agg1 agg2* plants exhibited enhanced growth and reduced defenses, *agg1 agg2 atg7/3* plants were able to grow and defend well at the same time. Transient FLS2 expression in *agg1 agg2* uncovered an anticipatory UPR-mediated response that appears hardwired to promote growth over defense and is actively repressed by G-proteins that directly interact with FLS2 at the ER. Although traditionally viewed as an adaptive response triggered by the accumulation of unfolded proteins in the ER, we show that UPR is also an anticipatory response that is activated well before the disruption of protein homeostasis. Our results provide the first evidence that Gβγ dimers

357 mediate growth-defense tradeoffs through UPR signaling. Furthermore, their signaling function
358 in the ER is independent of their canonical functions in the Gαβγ heterotrimers at the PM. The
359 ability to unlock or fine-tune growth-defense tradeoffs through UPR signaling provides a novel
360 strategy to combine plant traits in ways that can have practical applications in biotechnology and
361 agriculture.

362 A central premise underlying current views of growth-defense balance between BR and
363 flagellin signaling is that the defense-defense antagonism is largely unidirectional (favoring
364 growth over defense) and indirect (Lozano-Durán and Zipfel, 2015). This signaling architecture
365 presumably serves to prevent autoimmunity and severe growth retardation from prolonged
366 and/or de-regulated activation of immune receptors so that plants can excel in obtaining limited
367 resources from their competitors. The ability of *agg1 agg2* plants to grow robustly at the
368 expense of defense provides evidence that the growth-defense antagonism can be reversed to
369 promote faster activation of immune receptors and overcome domestication-related tradeoffs
370 against defensive traits. Furthermore, AGB1-AGG1/2 heterodimers bind directly to BRI1 and
371 FLS2 proteins at the ER membrane. In yeast and mammals, the binding of unfolded proteins to
372 IRE1 directly activates UPR under ER stress-inducing conditions (Gardner and Walter, 2011;
373 Karagöz et al., 2017). Similarly, the binding to BRI1 and FLS2 to AGB1-AGG1/2 may tune the
374 homeostatic functions of UPR under conditions that favor growth and are independent of ER
375 stress. Whether G-proteins in the ER also mediate growth-defense tradeoffs under defense-
376 inducing conditions remains to be tested.

METHODS

Plant materials and growth conditions. Surface-sterilized seeds of *Arabidopsis thaliana* accession Columbia-0 (Col-0) were stratified for at least 2 days and sown in 12- or 24-well microtiter plates sealed with parafilm. Each 12- or 24-well plate contained 12 and 5 seeds, respectively, with 1 and 0.5 mL of filter-sterilized 0.5X MS liquid (pH 5.7–5.8) [4.43 g/L Murashige and Skoog basal medium with vitamins (Murashige and Skoog, 1962) (Phytotechnology Laboratories, Shawnee Missions, KS), 0.05% (w/v) MES hydrate, 0.5% (w/v) sucrose], respectively. Alternatively, surface-sterilized and stratified seeds were sown on MS agar plates [0.5X MS, 0.75% (w/v) agar (PlantMedia, Chiang Mai, Thailand)] sealed with parafilm. Unless otherwise stated, sample-containing plates were placed on grid-like shelves over water trays on a Floralight cart (Toronto, Canada), and plants were grown at 21˚C and 60% humidity under a 12-hr light cycle (70–80 µE m^{-2} s^{-1} light intensity). Unless otherwise stated, media in microtiter plates were exchanged for fresh media on day 7. For bacterial infection experiments, *Arabidopsis* plants were grown on soil [3:1 mix of Fafard Growing Mix 2 (Sun Gro Horticulture, Vancouver, Canada) to D3 fine vermiculite (Scotts, Marysville, OH)] at 22˚C daytime/18˚C nighttime with 60% humidity under a 12-hr light cycle (100 µE m^{-2} s^{-1} light intensity). *Nicotiana benthamiana* plants were grown on soil [3:1 mix] on a Floralight cart at 22˚C under a 12-hr light cycle (100 µE m^{-2} s^{-1} light intensity) for 4 weeks.

The following Col-0 T-DNA insertion lines and mutants were obtained from the Arabidopsis Biological Resource Center (ABRC, Columbus, Ohio): *agb1-1* (CS3976), *agb1-2* (CS6535), *agg1-1c* (CS16550), *agg2* (SALK_039423), *agg1-1c/agg2-1* (CS16551), *atg7* (SAIL_11_H07), *fls2* (SAIL_691_C4).

401 **Vector construction and transformation.** To generate estradiol-inducible C-terminally tagged
402 *GFP* and *RFP* (*XVE:X-G/RFP*) and *35S:YFP-AGB1* DNA constructs, *attB* sites were added via
403 PCR-mediated ligation to the coding sequences of cDNAs, and the modified cDNAs were
404 recombined into pDONR221 entry vector and then into pABindGFP, pABindRFP (Bleckmann et
405 al., 2010) and pB7WGY2 (Karimi et al., 2002) destination vectors, according to manufacturer's
406 instructions (Gateway manual; Invitrogen, Carlsbad, CA). *XVE:AGG1-RFP, XVE:FLS2-RFP,*
407 and *35S:YFP-AGB1* constructs were introduced into *agg1-1c agg2-1* or *agb1-2* plants via
408 *Agrobacterium*-mediated floral dip method (Clough and Bent, 1998), and transformants were
409 selected on agar media containing 15 µg/mL hygromycin B (Invitrogen) or 15 µg/mL glufosinate
410 (Cayman Chemical, Ann Arbor, MI). Transgene expression was induced 48 hr (or 5-6 days for
411 growth assays) after elicitation with 20 µM β-estradiol (2 mM stock solution in DMSO; Sigma-
412 Aldrich, St. Louis, MO). Transient expression of *XVE:X-G/RFP* constructs in *Nicotiana*
413 *benthamiana* leaves was performed as previously described (Bleckman et al., 2010) with the
414 following modification: transformed *Agrobacterium* strains were grown in LB medium
415 supplemented with 50 µg/mL rifampicin, 30 µg/mL gentamycin, kanamycin 50 µg/mL and 100
416 µg/mL spectinomycin, in the absence of a silencing suppressor, to an OD_{600} of 0.7. Transgene
417 expression was induced 10 hr (for co-immunoprecipitation) and 4-8 hr (for microscopy) after
418 spraying with 20 µM β-estradiol and 0.1% Tween-20.
419
420 **BL-induced hypocotyl elongation.** Seedlings were grown on MS agar supplemented with 1 or
421 10 µM 24-epibrassinolide (BL; Phytotechnology Laboratories). Sample-containing agar plates
422 were placed vertically on a Floralight cart under a constant light cycle (140–180 µE m^{-2} s^{-1} light
423 intensity). Hypocotyl lengths were measured from images of 5-day-old seedlings using NIH
424 ImageJ.
425

426 **Flg22-induced seedling growth inhibition.** Three-day-old seedlings in 24-well microtiter
427 plates were elicited with water or 100 nM flg22 (QRLSTGSRINSAKDDAAGLQIA; Genscript,
428 Nanjing, China) for 6 days. Fresh weights were measured from 9-day-old seedlings that were
429 dried between paper towels for a few seconds.
430
431 **Flg22-induced Callose Deposition.** 9-day-old seedlings were elicited with 1 μM flg22 for 16-18
432 hr. Alternatively, 9-day-old seedlings were treated with DMSO, 100 nM BL, or 1 μM BL 6 hours
433 prior to flg22 elicitation. Callose deposition staining was performed as previously described
434 (Clay et al., 2009). Callose deposits were viewed on a Zeiss (Oberkochen, Germany)
435 AxioObserver D1 fluorescence microscope under UV illumination with Filter Set 49 (excitation
436 filter 365 nm; dichroic mirror 395 nm; emission filter 445/50 nm). Callose deposits were
437 quantified using NIH ImageJ.
438
439 **Flg22-induced MAPK activation.** 9-day-old seedlings were elicited with 100 nM flg22 for 5, 15,
440 and/or 30 min. MAPK activation assay was performed as previously described (Lawerence et
441 al., 2017). 20 μl of supernatant was loaded onto a 10% SDS-PAGE gel, and the separated
442 proteins were transferred to PVDF membrane (Millipore) and probed with phosphor-p44/p42
443 MAPK (Cell Signaling Technology, Danvers, MA) and MPK3 antibodies (Sigma-Aldrich, St.
444 Louis, MO) at 1:2000 dilution in 5% (w/v) nonfat milk in 1X PBS. The combined signal intensities
445 of phosphorylated MPK3/4/6 were quantified using NIH ImageJ and normalized to that of total
446 MPK3 (loading control).
447
448 **Total protein extraction, SDS-PAGE, and western blotting.** Total protein was extracted from
449 snap-frozen seedlings into 80 μL of extraction buffer [50 mM Tris-Cl (pH 7.5), 50 mM DTT, 4%
450 (w/v) SDS, 10% (v/v) glycerol] using a 5-mm stainless steel bead and ball mill (20 Hz for 3 min).
451 Samples were centrifuged briefly, incubated at 95˚C for 10 min, and centrifuged at 12,000 x g

for 8 min to precipitate insoluble material. Endo H treatment was performed as previously described (Lawrence et al., 2017). 5 or 10 µL of extract were loaded onto a 8.5% SDS-PAGE gel, and the separated proteins were transferred to PVDF membrane (Millipore, Billerica, MA), stained with Ponceau S for labeling of total protein (loading control), and probed with either BRI1 (Agrisera), FLS2 (antigen: CTKQRPTSLNDEDSQ; Genscript), RFP (MBL International, Woburn, MA), GFP (Roche, Basel, Switzerland), BIP (Enzo Life Sciences, Farmingdale, NY), PDI antibodies at 1:500 (BRI1), 1:1000 (FLS2, RFP, GFP) and 1:5000 (BIP, PDI) dilutions in 5% (w/v) nonfat milk in 1X PBS. Signal intensities of immuno-detected proteins were quantified using NIH ImageJ and normalized to that of loading control.

Aqueous 2-phase partitioning and immunoprecipitation. Microsomal membrane (MM) and plasma membrane (PM) proteins were isolated from 250 mg of snap-frozen plant tissue using Minute Plasma Membrane Protein Isolation Kit for Plants (Invent Biotechnologies, Plymouth, MN). Membrane protein pellets were extracted into 250 µL of extraction buffer [50 mM Tris-Cl, pH 7.5, 150 mM NaCl, 1% NP-40, 10% glycerol, 2 mM EDTA, 5 mM DTT, complete-mini protease inhibitor cocktail (Roche), 5 µM AEBSF] for 1 hr at 4˚C with rocking and clarified at 8,000 x g for 10 min. Twenty microliters of extract was set aside as input. Membrane proteins were immunoprecipitated with 2.5 µL of antibody for 4 hr at 4˚C with rocking followed by 25 µL of 50% slurry of Protein A/G magnetic beads (EMD Millipore, Burlington MA) for 1 hr at 4˚C with rocking, and washed 3x with 350 µL of wash buffer (50 mM Tris-Cl, pH 7.5, 150 mM NaCl). Enrichment of ER membrane proteins in the MM protein extracts was confirmed by western blotting using BIP antibody.

RNA isolation and quantitative PCR (qPCR). Total RNA was extracted into 1 mL of TRIzol reagent (Invitrogen) according to manufacturer's instructions. 2 µg of total RNA was reverse-transcribed with 3.75 µM random hexamers (Qiagen, Hilden, Germany) and 20 U of ProtoScript

II (New England Biolabs, Boston, MA). The resulting cDNA:RNA hybrids were treated with 10 U of DNase I (Roche) for 30 min at 37˚C, and purified on PCR clean-up columns (Macherey-Nagel, Düren, Germany). qPCR was performed with Kapa SYBR Fast qPCR master mix (Kapa Biosystems, Wilmington, MA) and CFX96 or CFX384 real-time PCR machine (Bio-Rad, Hercules, CA). The thermal cycling program is as follows: 95°C for 3 min; 45 cycles of 95°C for 15 sec and 53°C or 55˚C for 30 sec; a cycle of 95°C for 1 min, 53°C for 1 min, and 70°C for 10 sec; and 50 cycles of 0.5°C increments for 10 sec. Biological replicates of control and experimental samples, and three technical replicates per biological replicate were performed on the same 96- or 384-well PCR plate. Averages of the three Ct values per biological replicate were converted to differences in Ct values relative to that of control sample. Pfaffl method (Pfaffl 2001) and calculated primer efficiencies were used to determine the relative fold increase of the target gene transcript over the housekeeping *eIF4AI* gene transcript for each biological replicate. Primer sequences and efficiencies are listed in Supplementary Table 1.

Confocal microscopy. Live epidermal root cells of 5-day-old *Arabidopsis* seedlings and 4-week-old *N. benthamiana* leaves were imaged using a 40X 1.0 numerical aperture Zeiss water-immersion objective and a Zeiss LSM 510 Meta confocal microscopy system. GFP and RFP were excited with a 488-nm argon laser and 561-nm laser diode, respectively. GFP and RFP emissions were detected using a 500-550 nm and 575-630 nm filter sets, respectively. Plasmolysis was induced by 5-10 min treatment of *N. benthamiana* leaf strips with 0.8 mannitol, and co-localization of GFP/RFP-tagged proteins to Hechtian strands was made visible by over-exposing confocal images using ZEN software.

ER stress induction. For qPCR and western blots, 9-day-old seedlings were treated with 5 µg/mL tunicamycin (0.5 mg/mL stock solution in DMSO; Sigma-Aldrich) or solvent control

(DMSO) for 5 hr. For growth inhibition, seedlings were grown on MS agar supplemented with 0, 25, 50, and 100 ng/mL tunicamycin for 14 days.

Inhibition of protein translation and degradation. For BRI1 westerns, 5-day-old seedlings were treated with DMSO (mock) or 50 µM cycloheximide for 6 hr. For FLS2 westerns, 9-day-old seedlings were treated with 50 µM cycloheximide for 0, 2 and 16 hr. 9-day-old seedlings were also treated with DMSO (mock), 50 µM MG132 (50 mM stock solution in DMSO; Selleck Chemicals, Houston, TX), 20 µM E-64d (20 mM stock solution in DMSO; Cayman Chemical), and/or 2 µM concanamycin A (200 µM stock solution in DMSO; Santa Cruz Biotechnology) for 24 hr. For growth inhibition, 3-day-old seedlings were elicited with 100 nM flg22 or water for 2 days, and then treated with DMSO, 50 nM MG132, and/or 20 nM E-64d for 4 days.

Bacterial infection. Pathogen assays on 4- to 5-week-old adult leaves were performed as previously described (Chezem et al., 2017).

ACKNOWLEDGEMENTS

We thank N. Koizumi for *ire1a-2/ire1b-2* (SALK_018112, GABI_638B07) mutant, B. Bartel for *atg3* mutant, F. Ausubel for *bri1-116* mutant, R. Simon for pABindGFP and pABindRFP vectors, and C. Somerville for PDI antibody. The work was supported by T32 GM007223 (to J.C.M), T32 GM007499 (to S.A.L), Yale University Elizabeth Brown Fellowship (to T.C.), and Yale College Dean's Research Fellowship (to C.B.).

References

528 1. Adjobo-Hermans MJ, Goedhart J, Gadella TW Jr (2006) Plant G protein heterotrimers
529 require lipidation motifs of Gα and Gγ and do not dissociate upon activation. *J Cell Science*
530 119(Pt 24): 5087-5097.
531 2. Albrecht C, et al. (2012) Brassinosteroids inhibit pathogen-associated molecular pattern-
532 triggered immune signaling independent of the receptor kinase BAK1. *Proc Natl Acad Sci*
533 *USA* 109(1):303-308.
534 3. Belkhadir Y, et al. (2012) Brassinosteroids modulate the efficiency of plant immune
535 responses to microbe-associated molecular patterns. *Proc Natl Acad Sci USA* 109(1):297-
536 302.
537 4. Bao, Y, Howell SH (2017) The unfolded protein response supports plant development and
538 defense as well as responses to abiotic response. *Front Plant Sci* 8:344.
539 5. Bleckmann, A., *et al*. (2010). Stem cell signaling in Arabidopsis requires CRN to localize
540 CLV2 to the plasma membrane. *Plant Cell* **152**(1), 166-176.
541 6. Boudsocq M, et al. (2010) Differential innate immune signalling via Ca^{2+} sensor protein
542 kinases. *Nature* 464(7287):418-422.
543 7. Chakravorty D, Botella JR (2007) Over-expression of a truncated *Arabidopsis thaliana*
544 heterotrimeric G protein gamma subunit results in a phenotype similar to alpha and beta
545 subunit knockouts. *Gene* 393(1–2):163-170.
546 8. Chakravorty D, et al. (2011) An atypical heterotrimeric G-protein γ-subunit is involved in
547 guard cell K(+)-channel regulation and morphological development in *Arabidopsis thaliana.*
548 *Plant J* 67(5):840-851.
549 9. Chakravorty D, et al. (2015) Extra-large G proteins (XLGs) expand the repertoire of subunits
550 in *Arabidopsis* heterotrimeric G protein signaling. *Plant Physiol* 169(1):512-529.

10. Chen JG, et al. (2004) GCR1 can act independently of heterotrimeric G-protein in response to brassinosteroids and gibberellins in *Arabidopsis* seed germination. *Plant Physiol* 135(2):907-915.

11. Chen Y, Brandizzi F (2012) AtIRE1A/AtIRE1B and AGB1 independently control two essential unfolded protein response pathways in Arabidopsis. *Plant J* 69(2):266-277.

12. Chezem, W.R. *et al.* (2017). SG2-type R2R3-MYB transcription factor MYB15 controls defense-induced lignification and basal immunity in Arabidopsis. *Plant Cell* **29**(8), 1907-1926.

13. Clay, N.K. *et al.* (2009). Glucosinolate metabolites required for an Arabidopsis innate immune response. *Science* **323**(5910), 95-101.

14. Clough, S.J. & Bent, A.F. (1998). Floral dip: a simplified method for *Agrobacterium*-mediated transformation of *Arabidopsis thaliana. Plant J* **16**(6), 735-743.

15. Clouse SD, Langford M, McMorris TC (1996) A brassinosteroid-insensitive mutant in *Arabidopsis thaliana* exhibits multiple defects in growth and development. *Plant Physiol* 111(1996):671-678.

16. Deng Y, et al. (2011) Heat induces the splicing by IRE1 of a mRNA encoding a transcription factor involved in the unfolded protein response in Arabidopsis. *Proc Natl Acad Sci* 108(17):7247-7252.

17. Ding L, Pandey S, Assmann SM (2008) Arabidopsis extra-large G proteins (XLGs) regulate root morphogenesis. *Plant J* 53(2):248-263.

18. Dodds PN, Rathjen JP (2010) Plant immunity: towards an integrated view of plant-pathogen interactions. *Nat Rev Genet* 11(8):539-548.

19. Dupre DJ, et al. (2007) Dopamine receptor interacting protein 78 acts as a molecular chaperone for Gγ subunits prior to assembly with Gβ. *J Biol Chem* 282(18):13703-13715.

575 20. Fan M, et al. (2014) The bHLH transcription factor HBI1 mediates the trade-off between
576 growth and pathogen-associated molecular pattern-triggered immunity in *Arabidopsis. Plant*
577 *Cell* 26(2):828-841.
578 21. Gardner BM, Walter P (2011) Unfolded proteins are Ire1-activating ligands that directly
579 induce the unfolded protein response. *Science* 333(6051):1891-1894.
580 22. Giannotta M, et al. (2012) The KDEL receptor couples to Galpha(q/11) to activate Src
581 kinases and regulate transport through the Golgi. *EMBO J* 31(13):2869-2881.
582 23. Gomord V, et al. (1997) The C-terminal HDEL sequence is sufficient for retention of
583 secretory proteins in the endoplasmic reticulum (ER) but promotes vacuolar targeting of
584 proteins that escape the ER. *Plant J* 11(2):313-325.
585 24. Gómez-Gómez L, Boller T (2000) FLS2: an LRR receptor-like kinase involved in the
586 perception of the bacterial elicitor flagellin in *Arabidopsis*. *Mol Cell* 5(6):1003-1011.
587 25. González-García MP, et al. (2011) Brassinosteroids control meristem size by promoting cell
588 cycle progression in Arabidopsis roots. *Development* 138(5):849-859.
589 26. Hewavitharana T, Wedegaertner (2012) P.B. Non-canonical signaling and localizations of
590 heterotrimeric G proteins. *Cell Signal* 24(1):25-34.
591 27. Huot B, et al. (2014) Growth-defense tradeoffs in plants: a balancing act to optimize fitness.
592 *Mol Plant* 7(8):1267-1287.
593 28. Ishikawa A (2009) The *Arabidopsis* G-protein beta-subunit is required for defense response
594 against *Agrobacterium tumefaciens*. *Biosci Biotech Biochem* 73(1):47-52.
595 29. Janssens S, Pulendran B, Lambrecht BN (2014) Emerging functions of the unfolded protein
596 response in immunity. *Nat Immunol* 15(10):910-919.
597 30. Jiménez-Góngora T, Kim SK, Lozano-Durán R, Zipfel C (2015) Flg22-triggered immunity
598 negatively regulates key BR biosynthetic genes. *Front Plant Sci* 6:981.

599 31. Kamo K, Blowers A, McElroy D (2000) Effect of cauliflower mosaic virus 35S, actin, and
600 ubiquitin promoters on expression for a *bar-uidA* fusion gene in transgenic *Gladiolus* plants.
601 *In Vitro Cell Dev Biol Plant* 36(1):13-20.
602 32. Karagöz GE, et al. (2017) An unfolded protein-induced conformational switch activates
603 mammalian IRE1. *eLife* 6:e30700.
604 33. Karimi, M., Inzé, D. & Depicker, A. (2002). GATEWAY™ vectors for *Agrobacterium*-
605 mediated plant transformation. *Trends Plant Sci* **7**(5), 193-195.
606 34. Kaydamov C, Tewes A, Adler K, Manteuffel R (2000) Molecular characterization of cDNAs
607 encoding G protein alpha and beta subunits and study of their temporal and spatial
608 expression patterns in *Nicotiana plumbaginifolia* Viv. *Biochim Biophys Acta* 1491(1-3):143-
609 160.
610 35. Klayman LM, Wedegaertner PB (2017) Inducible inhibition of Gβγ reveals localization-
611 dependent functions at the plasma membrane and Golgi*. J Biol Chem* 292(5):1773-1784.
612 36. Klionsky DJ (2005) The molecular machinery of autophagy: unanswered questions. *J Cell*
613 *Sci* 118(Pt 1):7-18.
614 37. Kim SH, Kwon C, Lee JH, Chung T (2012) Genes for plant autophagy: Functions and
615 interactions. *Mol Cells* 34(5):413-423.
616 38. Koizumi N, et al. (2001) Molecular characterization of two Arabidopsis Ire1 homologs,
617 endoplasmic reticulum-located transmembrane protein kinases. *Plant Physiol* 127(3):949-
618 962.
619 39. Lawrence S.A., Ceserani, T., Clay, N.K. (2017). Assays to investigate the *N*-glycoslylation
620 state and function of plant pattern recognition receptors. *Methods Mol. Biol.* 1578: 61-79.
621 40. Lease KA, et al. (2001) A mutant Arabidopsis heterotrimeric G protein beta subunit affects
622 leaf, flower, and fruit development. *Plant Cell* 13(12):2631-2641.
623 41. Lee YRJ, Assmann SM (1999) *Arabidopsis thaliana* 'extra-large GTP-binding protein'
624 (AtXLG1): a new class of G-protein. *Plant Mol Biol* 40(1):55-64.

42. Liebminger E, et al. (2009) Class 1 alpha-mannosidases are required for *N*-glycan processing and root development in *Arabidopsis thaliana*. *Plant Cell* 21(12):3850-3867.

43. Li J, Chory J (1997) A putative leucine-rich repeat receptor kinase involved in brassinosteroid signal transduction. *Cell* 90(5):929-938.

44. Li J, et al. (2002) BAK1, an Arabidopsis LRR receptor-like protein kinase, interacts with BRI1 and modulates brassinosteroid signaling. *Cell* 110(2):213-222.

45. Liang X, et al. (2016) Arabidopsis heterotrimeric G proteins regulate immunity by directly coupling to the FLS2 receptor. *eLife* 5:e13568.

46. Liu J, et al. (2013) Heterotrimeric G proteins serve as a converging point in plant defense signaling activated by multiple receptor-like kinases. *Plant Physiol* 161(4):2146-2158.

47. Li, J-X, Srivastava R, Che P, Howell SH (2007) An endoplasmic reticulum stress response in *Arabidopsis* is mediated by proteolytic processing and nuclear relocation of a membrane-associated transcription factor, bZIP28. *Plant Cell* 19(12):4111-4119.

48. Lozano-Durán, R. *et al.* (2013) The transcriptional regulator BZR1 mediates trade-off between plant immunity and growth. *eLife* 3:e00983.

49. Lozano-Durán R, Zipfel C (2015) Trade-off between growth and immunity: role of brassinosteroids. *Trends Plant Sci* 20(1):12-19.

50. Marrari Y, Crouthamel M, Irannejad R, Wedegaertner PB (2007) Assembly and trafficking of heterotrimeric G proteins. *Biochemistry* 46(6):7665-7677.

51. Maruta N, et al. (2015) Membrane-localized extra-large G-Proteins and Gbetagamma of the heterotrimeric G proteins form functional complexes engaged in plant immunity in Arabidopsis. *Plant Physiol* 167(3):1004-1016.

52. Mason MG, Botella JR (2000) Completing the heterotrimer: Isolation and characterization of an *Arabidopsis thaliana* G protein gamma-subunit cDNA. *Proc Natl Acad Sci USA* 97(26):14784-14788.

650 53. Meng Z, Ruberti C, Gong Z, Brandizzi F (2017) CPR5 modulates salicylic acid and the
651 unfolded protein response to manage tradeoffs between plant growth and stress responses.
652 *Plant J* 89(3):486-501.
653 54. Miller JC, Chezem WR, Clay NK (2016) Ternary WD40 repeat-containing protein
654 complexes: evolution, composition and roles in plant immunity. *Front Plant Sci* 6:1108.
655 55. Murashige, T., Skoog, F. (1962). A revised medium for rapid growth and bio assays with
656 tobacco tissue cultures. *Physiol. Plant.* 15(3): 473-497.
657 56. Müssig C, Shin GH, Altmann T (2013) Brassinosteroids promote root growth in *Arabidopsis.*
658 *Plant Physiol* 133(3):1261-1271.
659 57. Nagashima Y, et al. (2014) Exogenous salicylic acid activates two signaling arms of the
660 unfolded protein response in Arabidopsis. *Plant Cell Physiol* 55(10):1772-1778.
661 58. Ohsumi Y (2001) Molecular dissection of autophagy: two ubiquitin-like systems. *Nat Rev Mol*
662 *Cell Biol* 2(3):211-216.
663 59. Oh-ye Y, Inoue Y, Moriyasu Y (2011) Detecting autophagy in Arabidopsis roots by
664 membrane-permeable cysteine protease inhibitor E-64d and endocytosis tracer FM4-64.
665 *Plant Signal Behav* 6(12):1946-1949.
666 60. Okuzaki A, et al. (2011) Estrogen-inducible GFP expression patterns in rice (*Oryza sativa* L.)
667 *Plant Cell Rep* 30(4):529-538.
668 61. Pandey S, Chen JG, Jones AM, Assmann SM (2006) G-protein complex mutants are
669 hypersensitive to abscisic acid regulation of germination and postgermination development.
670 *Plant Physiol* 141(1):253-256.
671 62. Peng Y, et al. (2018) BRI1 and BAK1 interact with G proteins and regulate sugar-responsive
672 growth and development in *Arabidopsis. Nat Commun* 9(1):1522.
673 63. Pfaffl, M.W. (2001). A new mathematical model for relative quantification in real-time RT-
674 PCR. *Nucleic Acids Res.* 29(9): e45.

675 64. Pu Y, Bassham DC (2013) Links between ER stress and autophagy in plants. *Plant Signal*
676 *Behav* 8(6):e24297.
677 65. Rivas-San Vicente M, Plasencia J (2011) Salicylic acid beyond defence: its role in plant
678 growth and development. *J Exp Bot* 62(10):3321-3338.
679 66. Ruberti C, Brandizzi F (2014) Conserved and plant-unique strategies for overcoming
680 endoplasmic reticulum stress. *Front Plant Sci* 5:69.
681 67. Smith MH, Ploegh HL, Weissman JS (2011) Road to ruin: targeting proteins for degradation
682 in the endoplasmic reticulum. *Science* 334(6059):1086-1090.
683 68. Spoel SH, Dong X (2008) Making sense of hormone crosstalk during plant immune
684 responses. *Cell Host Microbe* 3(6):384-351.
685 69. Thung L, Trusov Y, Chakravorty D, Botella JR (2012) G gamma1+G gamma2+G
686 gamma3=G beta: the search for heterotrimeric G-protein gamma subunits in *Arabidopsis* is
687 over. *J Plant Physiol* 169(5):542-545.
688 70. Torres MA, et al. (2013) Functional interplay between Arabidopsis NADPH oxidases and
689 heterotrimeric G protein. *Mol Plant-Microbe Interact* 26(6):686-694.
690 71. Trusov Y, et al. (2006) Heterotrimeric G proteins facilitate *Arabidopsis* resistance to
691 necrotrophic pathogens and are involved in jasmonate signaling. *Plant Physiol* 140(1):210-
692 220.
693 72. Trusov Y, et al. (2007) Heterotrimeric G Protein gamma subunits provide functional
694 selectivity in Gβγ dimer signaling in Arabidopsis. *Plant Cell* 19(4):1235-1250.
695 73. Ullah H, et al. (2001) Modulation of cell proliferation by heterotrimeric G protein in
696 Arabidopsis. *Science* 292(5524):2066-2069.
697 74. Ullah H, et al. (2003) The beta-subunit of the Arabidopsis G protein negatively regulates
698 auxin-induced cell division and affects multiple developmental processes. *Plant Cell*
699 15(2):393-409.

700 75. Wang S, Narendra S, Fedoroff N (2007) Heterotrimeric G protein signaling in the
701 Arabidopsis unfolded protein response. *Proc Natl Acad Sci USA* 104(10):3817-3822.
702 76. Wedegaertner PB (1998) Lipid modifications and membrane targeting of G alpha. *Biol*
703 *Signals Recept* 7(2):125-135.
704 77. Weiss CA, White E, Huang H, Ma H (1997) The G protein alpha subunit (G-alpha1) is
705 associated with the ER and the plasma membrane in meristematic cells of *Arabidopsis* and
706 cauliflower. *FEBS Lett* 407(3):361-367.
707 78. Yoshimoto K, et al. (2004) Processing of ATG8s, ubiquitin-like proteins, and their
708 deconjugation by ATG4 are essential for plant autophagy. *Plant Cell* 16(11):2967-2983.
709 79. Zhang T, et al. (2018) *Arabidopsis* G-protein beta subunit AGB1 interacts with BES1 to
710 regulate brassinosteroid signaling and cell elongation. *Front Plant Sci* 8:2225.
711 80. Zhang W, He SY, Assmann SM (2008) The plant innate immunity response in stomatal
712 guard cells invokes G-protein-dependent ion channel regulation. *Plant J* 56(6):984-996.
713 81. Zeng Q, Wang X, Running MP (2007) Dual lipid modification of Arabidopsis G gamma-
714 subunits is required for efficient plasma membrane targeting. *Plant Physiol* 143(3):1119-
715 1131.
716 82. Zhu H, et al. (2009) *Arabidopsis* extra large G-protein 2 (XLG2) interacts with the G beta
717 subunit of heterotrimeric G protein and functions in disease resistance. *Mol Plant* 2(3):513-
718 525.

719

720

721 **Figure legends**

722 **Figure 1. Increased BRI1 signaling contributes to enhanced growth of *agg1 agg2* mutant.**
723 (*A*) Growth pictures of 4-week-old and 6-week-old plants. White arrows indicate flowering
724 stems. White bars represent 10 cm. (*B*) Time course of growth and BRI1 protein expression.
725 Asterisks indicate significant differences from WT (P-value <0.05, two-tailed t test) Data

represent mean ± SD of three replicates of five seedlings. FW, fresh weight. (*C*) Growth analysis of 9-day-old plants. (*D*) Immunoblot analysis of BRI1 protein in untreated 6-day-old plants (left) and 9-day-old plants pretreated with 20 µM β-estradiol for 60 hr (right). Asterisks indicate non-specific protein bands. (*E*) BRI1 protein expression in 5.5-day-old plants in response to DMSO (mock) or 50 µM cycloheximide for 6 hr. Data in (*C*–*E*) represent mean ± SD of three replicates of twelve seedlings. Different letters in (*C*–*E*) indicate significant differences (*P*-value <0.05, two-tailed *t* test).

Figure 2. Increased FLS2 turnover contributes to enhanced growth of *agg1 agg2* mutant under defense-inducing conditions. (*A*) Growth inhibition analysis of 9-day-old plants pretreated with 20 µM β-estradiol and water (control) or 100 nM flg22 for 6 days. Data represent mean ± SD of four (*fls2*) or five (all others) replicates of five seedlings. (*B*–*C*) Immunoblot analysis of FLS2 protein in untreated (*B*, top) and β-estradiol-pretreated (*B*, bottom) 9-day-old plants. Asterisks indicate non-specific protein bands. Data in (*C*) represent mean ± SD of six (left) and three (right) replicates of twelve seedlings. (*D*) Time course of FLS2 protein expression in 9-day-old plants in response to 50 µM cycloheximide. Data represent mean ± SD of three replicates of twelve seedlings. Different letters in (*A* and *C*–*D*) indicate significant differences (*P*-value <0.05, two-tailed *t* test).

Figure 3. Growth and defense are uncoupled in *agg1 agg2* mutant. (*A*) qPCR analysis of MAPK-activated defense genes *CYP82C2* and *CYP81F2* in 9-day-old plants pretreated with water (mock), 1 µM 24-epibrassinolide (BL), and/or 100 nM flg22 for 3 hr. Data represent mean ± SD of four replicates of twelve seedlings. (*B*) Callose deposition analysis of 9-day-old plants pretreated with DMSO (control), 0.1 µM or 1 µM BL for 6 hr and then elicited with 1 µM flg22 for 16-18 hr. Data represent mean ± SE of fifteen replicates. (*C*) Growth analysis of 9-day-old

plants pretreated with DMSO (mock), 100 nM flg22, and/or 100 nM BL for 6 days. Data represent mean ± SD of five replicates of five seedlings. Different letters in (*A*–*C*) indicate significant differences (*P*-value <0.05, two-tailed *t* test).

Figure 4. AGG1 and AGG2 are involved in UPR signaling. (*A*) Growth inhibition analysis of 14 day-old plants in response to 0 (control), 25, 50 and 100 ng mL^{-1} tunicamycin. Data represent mean ± SD of five replicates of five seedlings. Asterisks indicate significant differences from WT; double asterisks indicate significant differences from WT, *agb1* and *ire1a ire1b*. (*B*) qPCR analysis of UPR-activated genes in 9-day-old seedlings pretreated with 5 µg mL^{-1} tunicamycin (+Tn) or DMSO (-Tn) for 5 hr. Data represent mean ± SD of four replicates of twelve seedlings. Single dagger indicates significant differences from WT; double daggers indicate significant differences from -Tn samples (*P*-value <0.05, two-tailed *t* test; FDR < 0.5).

Figure 5. AGB1-AGG1/2 interact with FLS2 at the ER membrane. (*A*) Co-localization of AGG1 with AGB1 and FLS2 at the ER membrane in transfected *N. benthamiana* leaves pretreated with 20 µM β-estradiol for 4-8 hr. HDEL is an ER marker. White bars represent 20 µm. (*B*) Immunoprecipitation (IP) of AGG1-GFP and co-immunoprecipitation (Co-IP) of FLS2-RFP from plasma membrane (PM) and microsomal membrane (MM) protein extracts of transfected *N. benthamiana* leaves pretreated with 20 µM β-estradiol for 10 hr. BIP is an ER membrane-associated protein in the absence of ER stress. (*C*) IP of AGG1-RFP and YFP-AGB1 and Co-IP of native FLS2 from PM and MM protein extracts of 9-day-old *agg1 agg2/XVE:AGG1-RFP* pretreated with 20 µM β-estradiol for 48 hr and untreated *agb1/35S:YFP-AGB1* plants.

Figure 6. Combination of *agg1 agg2* and *atg7/3* promotes robust growth and defense. (*A*) Growth inhibition analysis of 9-day-old plants pretreated with water (control) or 100 nM flg22 for

777 6 days. Data represent mean ± SD of four (*fls2*) or five (all others) replicates of five seedlings.
778 (*B*) Immunoblot analysis of FLS2 protein in 9-day-old plants. Data represent mean ± SD of six
779 replicates of twelve seedlings. (*C*) Growth analysis of 9-day-old plants. Data represent mean ±
780 SD of four (*fls2*) or five (all others) replicates of five seedlings. (*D*) Growth analysis of bacterial
781 pathogen *Pto* DC3000 in 5-week-old surface-inoculated leaves. Data represent mean ± SD of
782 six replicates. Different letters in (*A*–*D*) indicate significant differences (*P*-value <0.05, two-tailed
783 *t* test).
784
785 **Figure 7. UPR is hardwired to promote FLS2 protein degradation in the absence of ER**
786 **stress.** (*A*) Immunoblot analysis of FLS2 protein in 9-day-old *agg1 agg2/XVE:FLS2* lines
787 pretreated with DMSO (mock; left) or 20 µM β-estradiol (right) for 48 hr. Asterisks indicate non-
788 specific protein bands. Data represent mean ± SD of three replicates of twelve seedlings. (*B*)
789 FLS2 protein expression analysis of 6.5-day-old seedlings pretreated with 20 µM β-estradiol for
790 two days and then treated with DMSO (mock) or 20 µM E-64d and 2 µM Concanamycin A (Con
791 A) for 1.5 days. Data represent mean ± SE of four replicates of twelve seedlings. Different
792 letters in (*A*–*B*) indicate significant differences (*P*-value <0.05, two-tailed *t* test). (*C*) Proposed
793 function of G-protein dimers in UPR under growth-inducing conditions. AGB1-AGG1/2 dimers
794 mediate growth-defense tradeoffs between BL and flagellin signaling by interacting with nascent
795 FLS2 proteins at the ER membrane and inhibiting their autophagic degradation either through
796 signaling or sequestration. G-proteins also interact with nascent BRI1 proteins on the ER
797 membrane to repress their biogenesis through an unknown mechanism.
798
799
800 **Supplementary Figure Legends**
801 **Supplementary figure S1.** (*A*–*B*) Growth phenotypes of 5-week-old (*A*) and 8-week-old (*B*)
802 *atg7* and *agg1 agg2 atg7* plants (left) and *atg3* and *agg1 agg2 atg3* plants (right) relative to *WT*

and *agg1 agg2* plants. Growth phenotypes of 5-week-old (*A*) *agb1 atg7* and *agb1 atg3* plants are also included.

Supplemental figure S2. (*A*) Immunoblot analysis of BRI1 protein in 5-day-old WT, *agg1 agg2, agb1, ire1a ire1b*, *fls2*, and *bri1* plants. Asterisks indicate non-specific protein bands. FW, fresh weight. (*B*) Time course of *BRI1* gene expression in 9-day-old *WT, agg1 agg2* and *agb1* plants. Shading indicates night time. Data represent mean ± SD of 4 replicates of 12 seedlings. Different letters in (*A*–*B*) indicate significant differences (*P*-value <0.05, two-tailed *t* test).

Supplementary figure S3. (*A*) Growth curves of WT (left) and *agg1 agg2* (right) plants in response to water (mock/control), 100 nM flg22 or 1 µM flg22 starting at three days post-germination. Data represent mean ± SD of four replicates of five seedlings. (*B*) Growth inhibition curves of WT and *agg1 agg2* plants in response to water (control) or 1 µM flg22 starting at three days post-germination. Data represent mean ± SD of five replicates of five seedlings. Asterisks indicate significant differences from WT (*P*-value <0.05, two-tailed *t* test). (*C*) Time course of FLS2 protein expression in 9-day-old WT and *agg1 agg2*. Data represent mean ± SD of three replicates of twelve seedlings. Asterisks indicate significant differences from WT (*P*-value <0.05, two-tailed *t* test). Shading indicates night time. (*D*) Time course of *FLS2* gene expression in 9-day-old WT, *agg1*, and *agb1* plants. Shading indicates night time. Data represent mean ± SD of four replicates of twelve seedlings. Different letters indicate significant differences (*P*-value <0.05, two-tailed *t* test). (*E*) Immunoblot analysis of FLS2 protein from plasma membrane (PM) and microsomal membrane (MM) protein extracts of 9-day-old seedlings. Plants in the top panel were pretreated with 20 µM β-estradiol for 48 hr. Numbers under immunoblots indicate FLS2 signal intensities normalized to those of ER membrane-associated BIP and relative to WT.

828 **Supplementary figure S4.** (*A*–*C*) Immunoblot analysis of activated MAPKs in 9-day-old WT,
829 *agg1 agg2, agb1, agg1, agg2, fls2, and agg1 agg2/XVE:AGG1-RFP* lines in response to 100
830 nM flg22 for 5, 15, and/or 30 min. Numbers under immunoblots indicate combined
831 phosphorylated MPK3/4/6 signal intensities normalized to those of total MPK3 (loading control)
832 and relative to WT. Plants in (*C*) were pretreated with 20 µM β-estradiol for 48 hr.
833
834 **Supplementary figure S5.** Callose deposition analysis of 9-day-old WT, *agg1 agg2*, *agg1*
835 *agg2/XVE:AGG1-RFP*, *agb1, agb1/35S:YFP-AGB1,* and *fls2* plants in response to water
836 (control) or 1 µM flg22 for 16-18 hr. Plants on the left side of the graph were pretreated with 20
837 µM β-estradiol for 48 hr. Data represent mean ± SE of 14 (*agb1/35S:YFP-AGB1* #1) and 25 (all
838 others) replicates. Different letters indicate significant differences (*P*-value <0.05, two-tailed *t*
839 test).
840
841 **Supplementary figure S6.** (*A*–*C*) Hypocotyl elongation analysis of 5-day-old WT, *agb1*,
842 *agb1/35S:YFP-AGB1, agg1 agg2*, *agg1 agg2/XVE:AGG1-RFP, agg1, agg2, agg3,* and *agg1*
843 *agg2 agg3* plants in response to 0 (control), 1 µM 24-epibrassinolide (BL) (*A*) or 10 µM BL (*B*-*C*)
844 for 5 days. Plants in (*B*, right) were additionally pretreated with 20 µM β-estradiol for 48 hr.
845 Dashed lines indicate locations of hypocotyl-root junction in each plant. Data in (*A*–*C*) represent
846 mean ± SD of six replicates. Different letters indicate significant differences (*P*-value <0.05, two-
847 tailed *t* test).
848
849 **Supplementary figure S7.** Immunoblot analysis of ER chaperone and folding proteins BIP and
850 PDI in 9-day-old WT, *agg1 agg2, agb1, ire1a ire1b,* and *fls2* plants treated with DMSO (mock)
851 or 5 µg mL^{-1} tunicamycin for 5 hr.
852

Supplementary figure S8. (*A*) Co-localization of AGG1 with FLS2 and AGB1 at the PM. (*B*) Co-localization of AGG1 with FLS2 at plasmolysis-induced Hechtian strands (indicated by arrowheads). (*C*) Co-localization of AGG1-RFP to reticulate structures in 5-day-old *agg1 agg2/XVE:AGG1-RFP* plants pretreated with 20 μM β-estradiol for 48 hr. (*D*) Co-localization of BRI1 with AGG1 and AGB1 at the ER membrane. HDEL is an ER marker. Experiments in (*A, B, D*) were performed on transfected *N. benthamiana* leaves pretreated with 20 μM β-estradiol for 4 hr. White bars in (*A*–*D*) represent 20 μm.

Supplementary figure S9. Immunoprecipitation (IP) of AGG1-GFP and AGB1-GFP (indicated by arrowheads) and co-immunoprecipitation (Co-IP) of BRI1-RFP from PM and MM protein extracts of transfected *N. benthamiana* leaves pretreated with 20 μM β-estradiol for 10 hr. BIP is an ER membrane-associated protein in the absence of ER stress.

Supplementary figure S10. (*A*) Immunoblot analysis of FLS2 protein in 9-day-old WT and *agg1 agg2* plants pretreated with DMSO, 50 μM MG132, 20 μM E-64d, and/or 2 μM Concanamycin A (Con A) for 24 hr. Data represent mean ± SD of three replicates of twelve seedlings. (*B*) Two independent growth inhibition analyses of 9-day-old plants pretreated with water (control) or 100 nM flg22 for 2 days and then with DMSO (mock), 50 nM MG132, and/or 20 nM E-64d for 4 days. Data represent mean ± SD of five replicates of five seedlings. Asterisks indicate significant differences from WT (*P*-value <0.05, two-tailed *t* test). (*C*) Two independent growth analyses of 9-day-old WT and *agg1 agg2* plants pretreated with DMSO (mock), 50 nM MG132 and/or 20 nM E-64d. Data represent mean ± SD of five replicates of five seedlings.

Supplementary figure S11. (*A*) Immunoblot analysis of FLS2 proteins in 9-day-old WT*, mns1 mns2 mns3, agg1 agg2, atg7, agg1 agg2 atg7* plants. Total protein extracts were treated with citrate buffer (mock) or 1,000 U of Endoglycosidase H (Endo H) for 1.5 hr prior to separation on

879 SDS-PAGE gel. Black and red arrowheads indicate FLS2 protein bands that were treated with
880 citrate buffer and Endo H, respectively. (*B*) Immunoblot analysis of activated MAPKs in 9-day-
881 old WT*, atg7, agg1 agg2 atg7, atg3,* and *agg1 agg2 atg3* plants in response to 100 nM flg22 for
882 10 min.
883
884 **Supplementary figure S12.** (*A*) Growth analysis of bacterial pathogen *Pto* DC3000 in 5-week-
885 old surface-inoculated leaves of WT*, atg7, atg3, agb1 atg7, agb1 atg3, agb1*, and *fls2* plants.
886 Data represent mean ± SD of 6 replicates. Different letters indicate significant differences (*P*-
887 value <0.05, two-tailed *t* test). (*B*) Growth phenotypes of 10-week-old *atg7* and *agb1 atg7* plants
888 (top) and *atg3* and *agb1 atg3* plants (bottom) relative to WT and *agb1* plants.
889
890 **Supplementary figure S13.** Growth analysis of *agg1 agg2/XVE:FLS2* lines. Data represent
891 mean ± SD of five replicates of five seedlings. Different letters indicate significant differences (*P*-
892 value <0.05, two-tailed *t* test). FW, fresh weight.
893
894 **Supplementary table S14.** qPCR primer sequences and efficiencies.

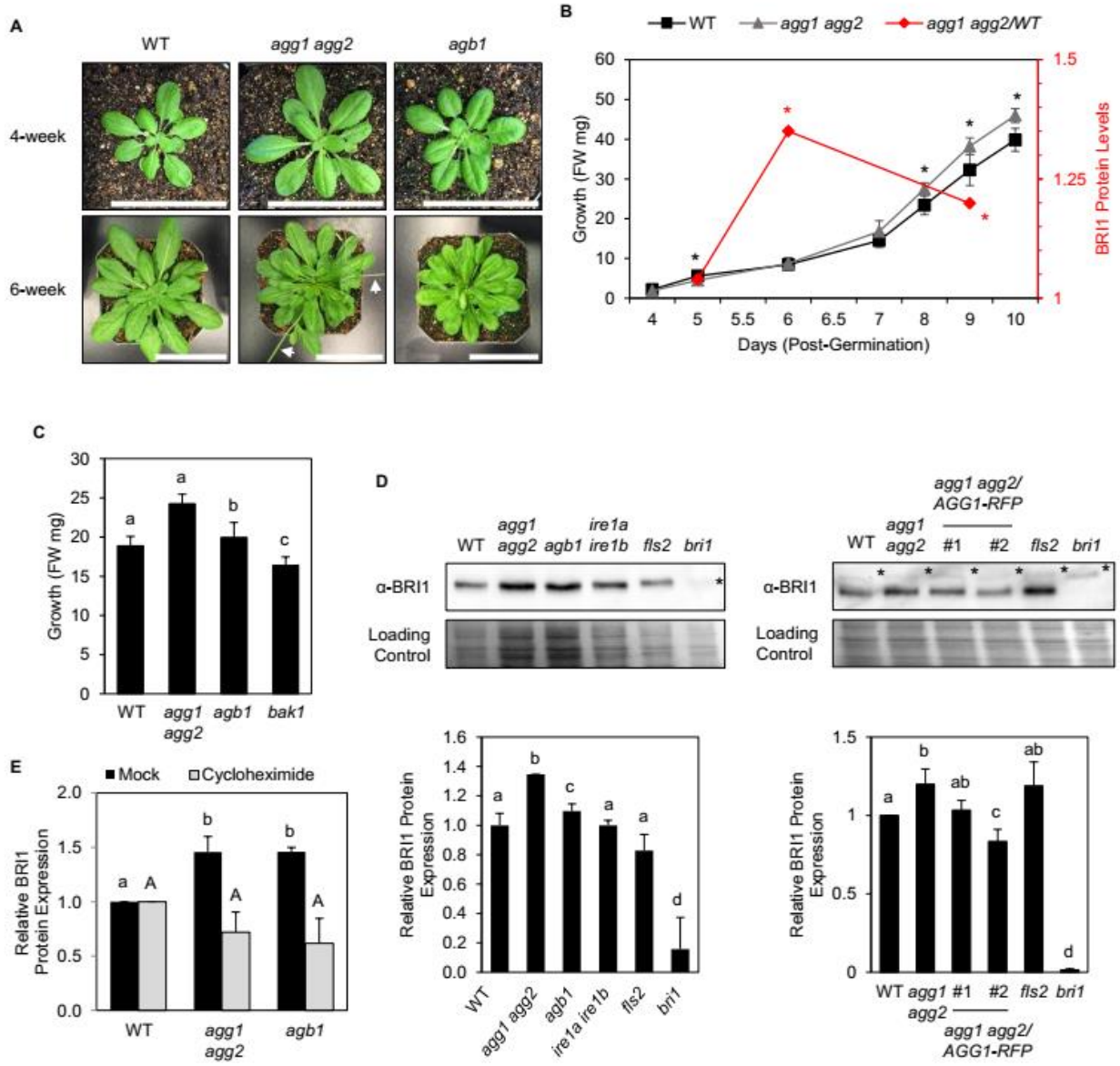

Figure 1. Increased BRI1 signaling contributes to enhanced growth of *agg1 agg2* mutant.

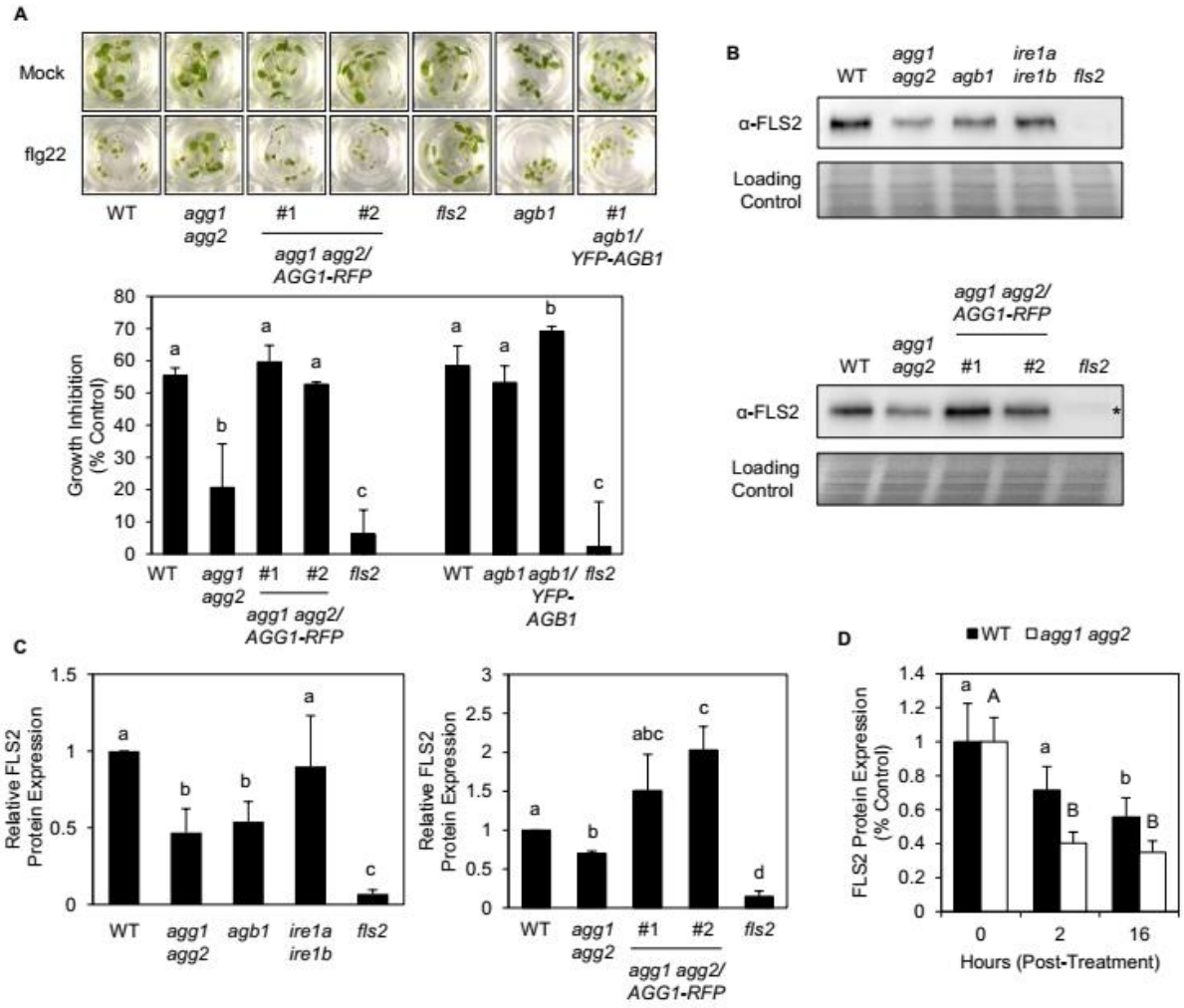

Figure 2. Increased FLS2 turnover also contributes to enhanced growth of *agg1 agg2* mutant under defense conditions.

898

899

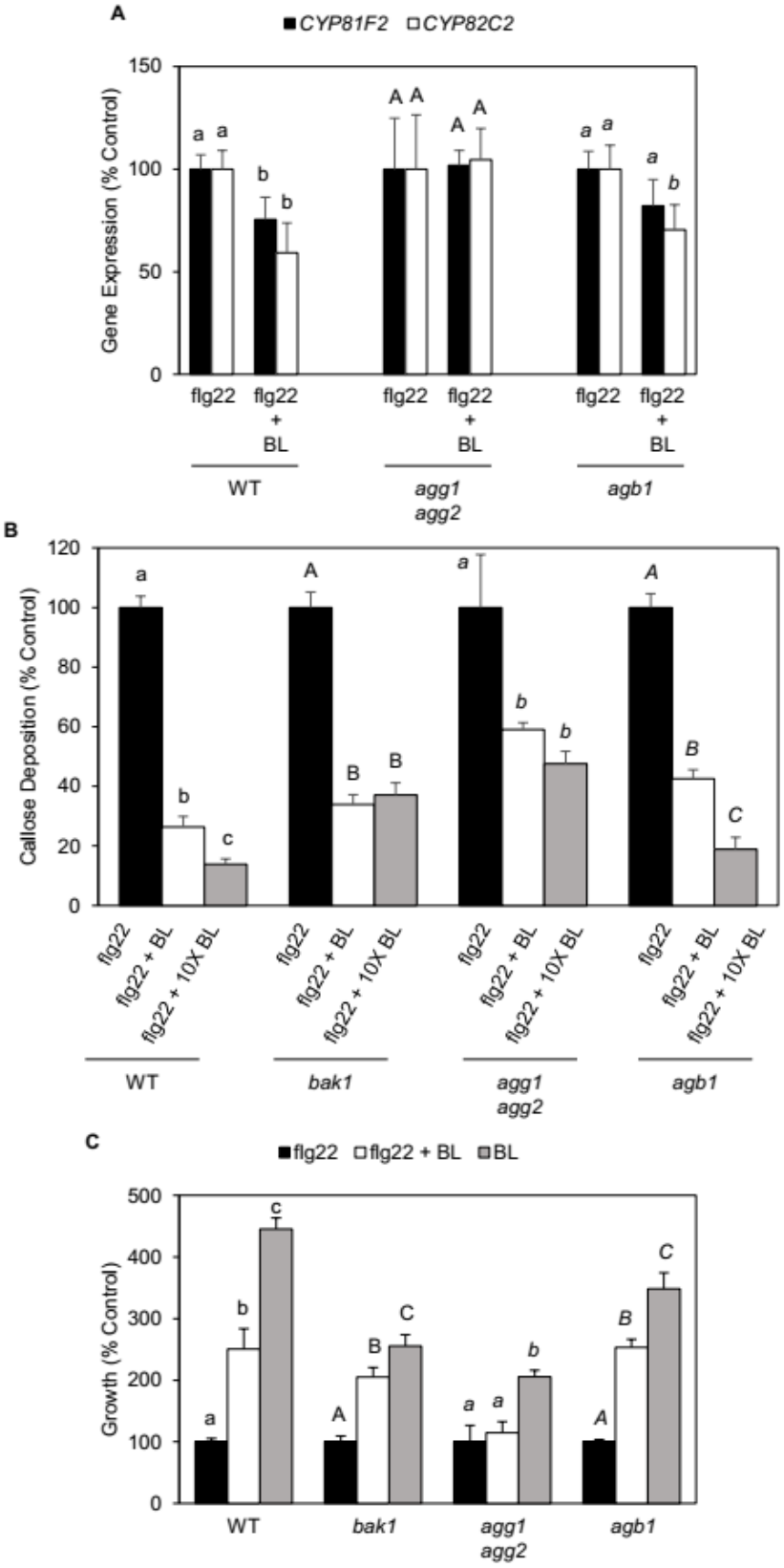

Figure 3. Growth and defense are uncoupled in *agg1 agg2* mutant.

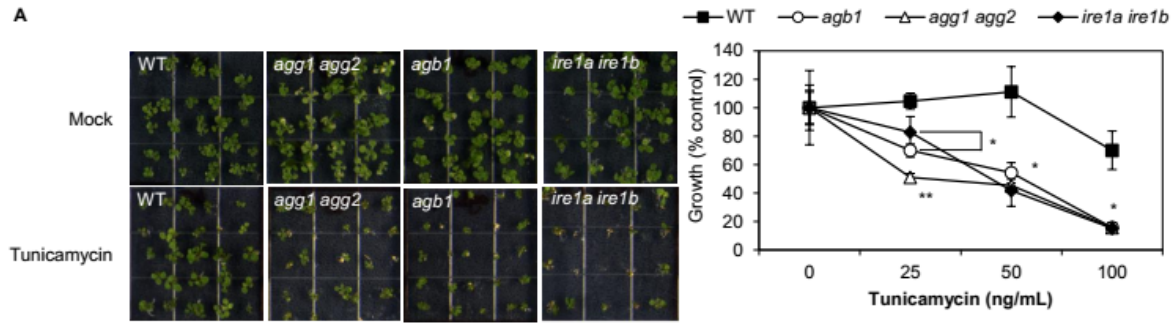

B

Relative Gene Expression

Geno type	*AGG1*		*AGG2*		*AGB1*		*IRE1A*		*IRE1B*		*BIP3*		*bZIP60s*	
	- Tn	+ Tn	- Tn	+ Tn	- Tn	+ Tn	- Tn	+ Tn	- Tn	+ Tn	-Tn	+ Tn	- Tn	+ Tn
WT	1.00	1.48‡	1.00	1.24‡	1.00	1.88‡	1.00	2.07‡	1.00	1.39‡	1.00	1.29	1.00	14.45‡
agg1 agg2	0.72	0.45†	0.83	1.10‡	1.05	1.64‡	1.11	2.48‡	1.24†	1.45‡	0.76	3.53†‡	1.14	16.67‡
agb1	1.26†	1.25	0.96	1.24	0.34†	0.50†	0.98	2.03‡	0.99	1.51	0.71	1.29	1.25	13.68‡
WT	1.00	1.49	1.00	0.99	1.00	1.58‡	1.00	1.53	1.00	1.84‡	1.00	1.29	1.00	8.37‡
Ire1a ire1b	0.74†	1.06†‡	0.67	1.13‡	0.77	1.10†	0.01†	0.03†	0.30†	0.31†	0.98	1.20	0.73†	3.39†‡

Figure 4. AGB1-AGG1/2 mediate a UPR-associated growth-defense tradeoff.

901

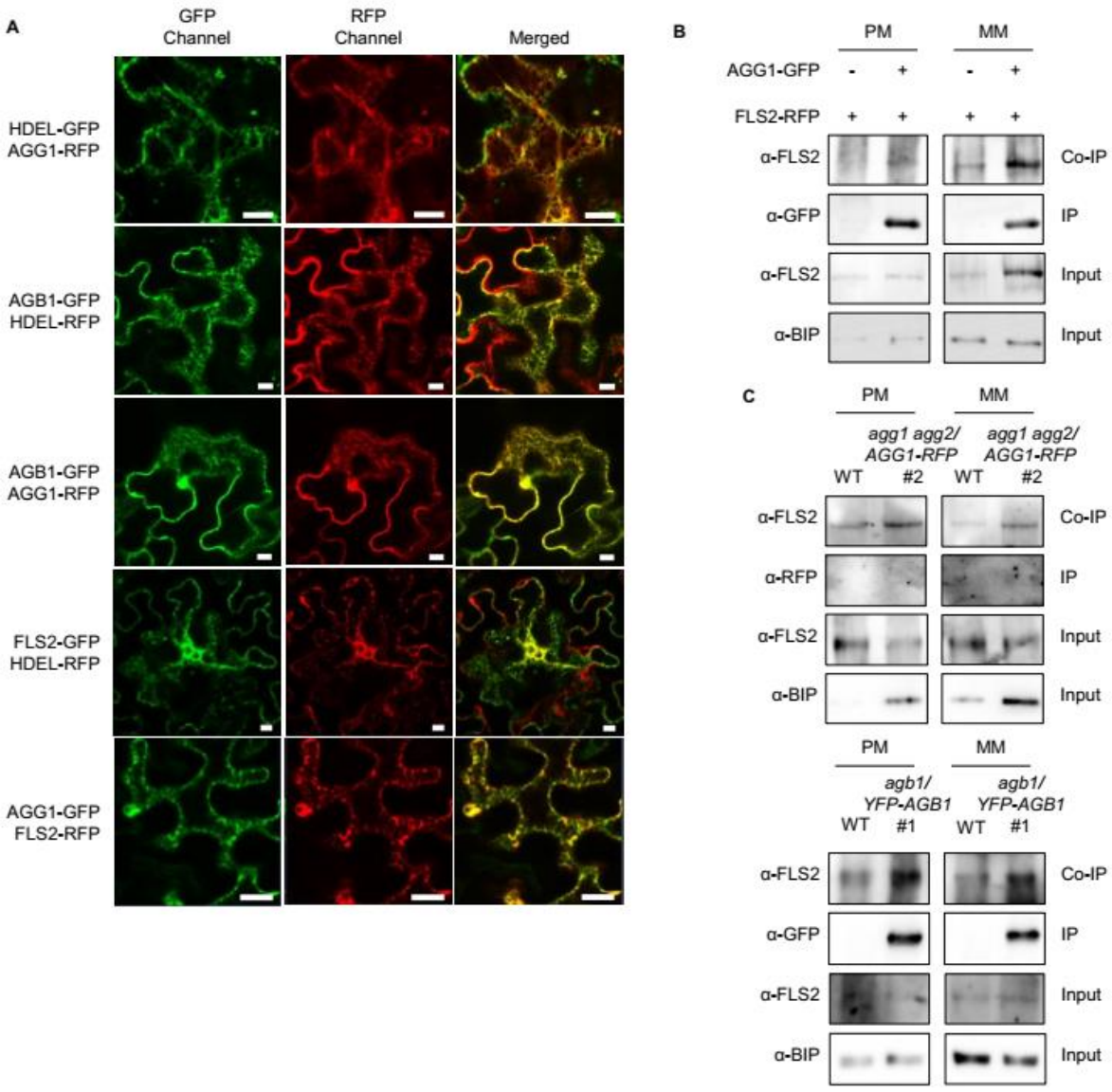

Figure 5. AGB1-AGG1/2 interact with nascent FLS2 protein at the ER membrane.

902

903

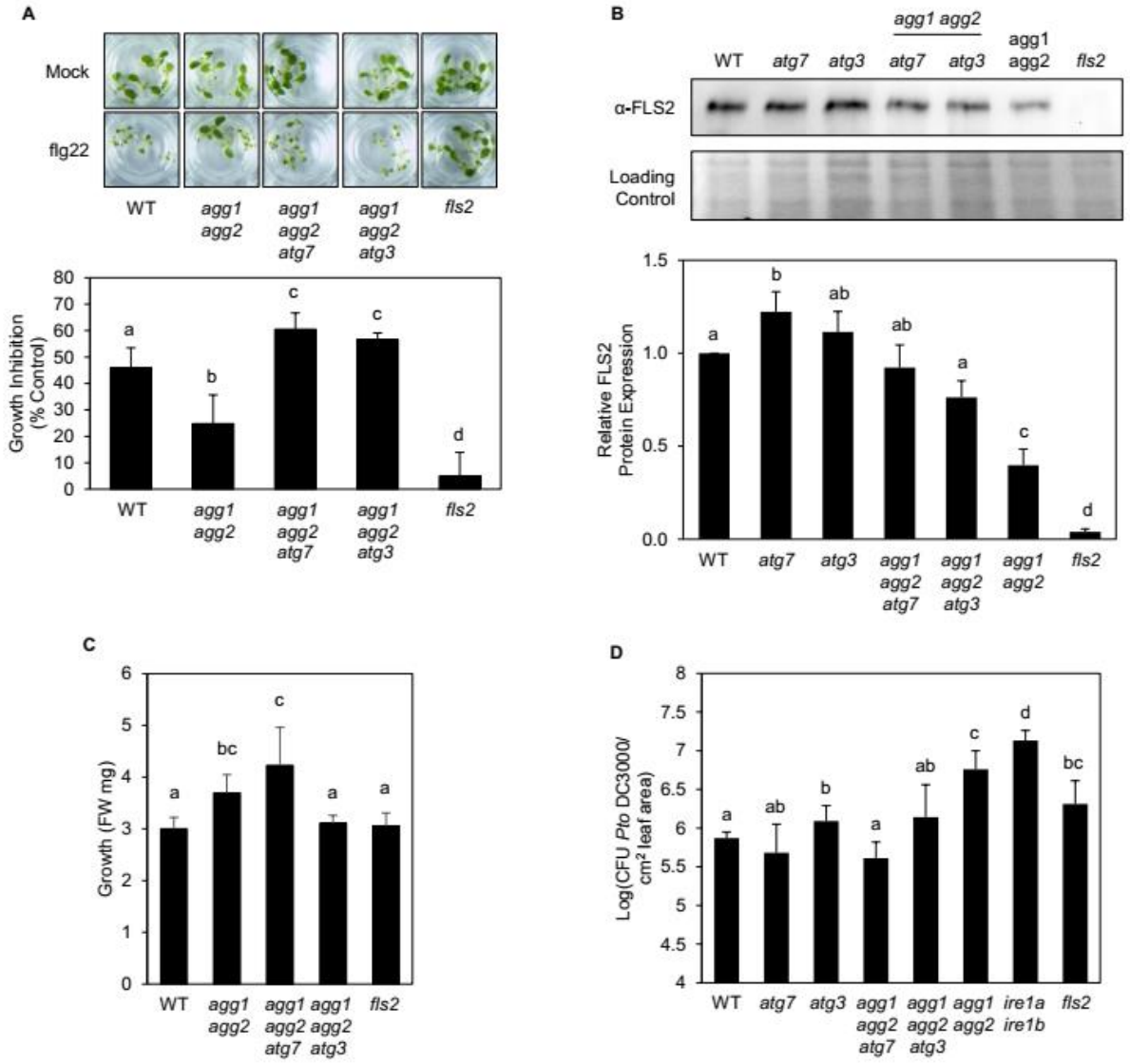

Figure 6. Combination of *agg1 agg2* and *atg7/3* promotes robust growth and defense.

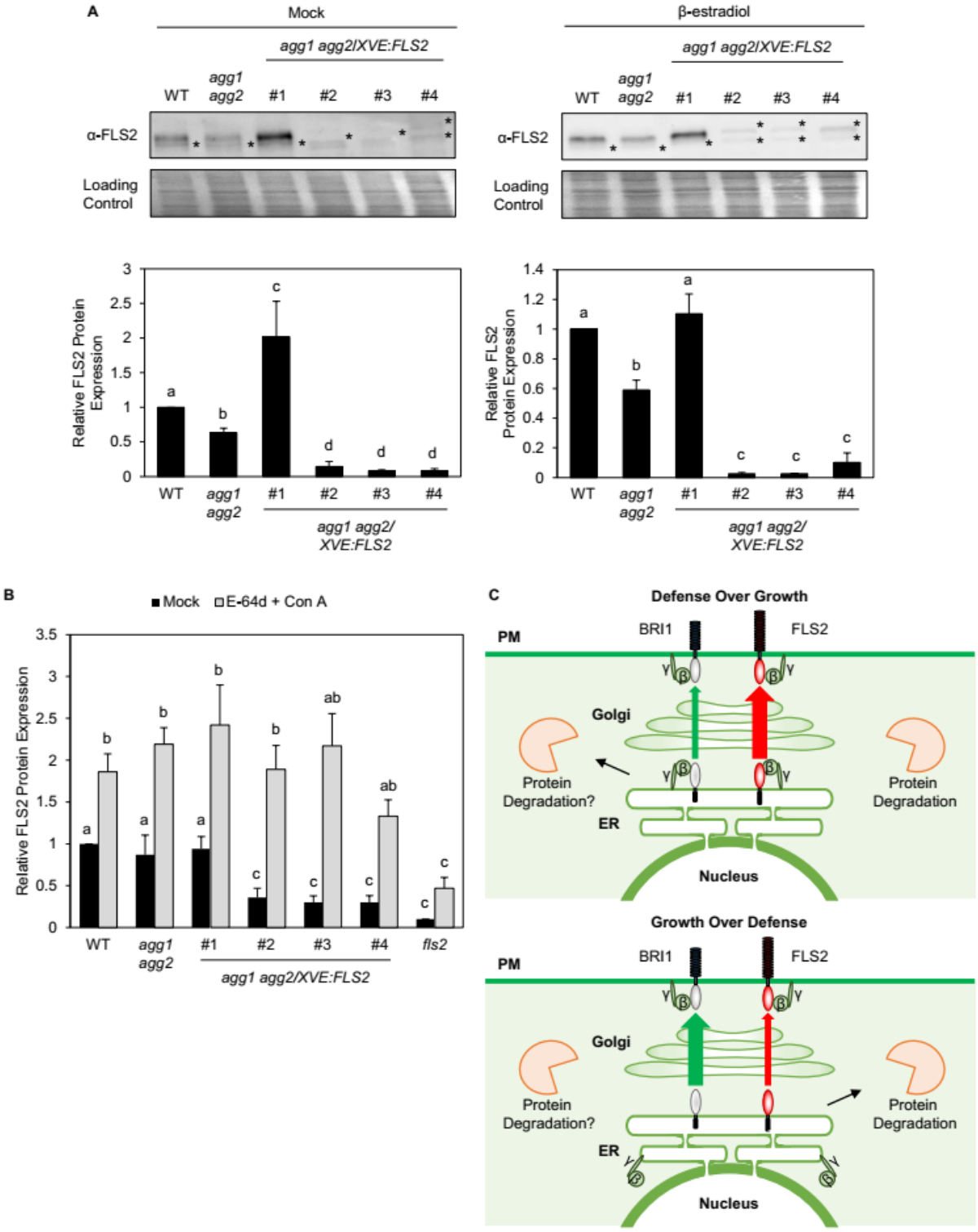

Figure 7. UPR is hardwired to promote FLS2 protein degradation under normal growth conditions.

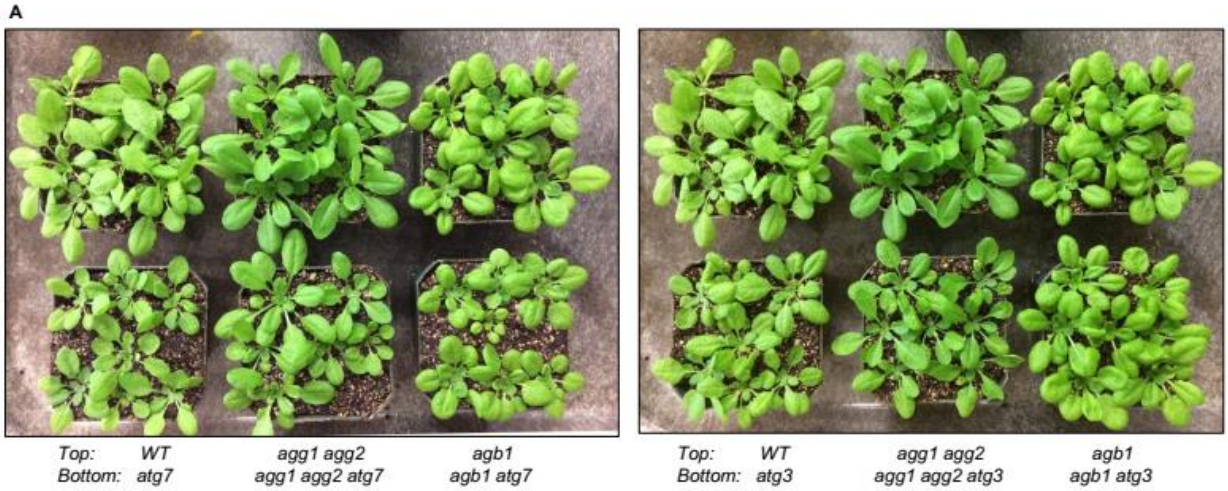

Supplementary Figure S1.

908

909

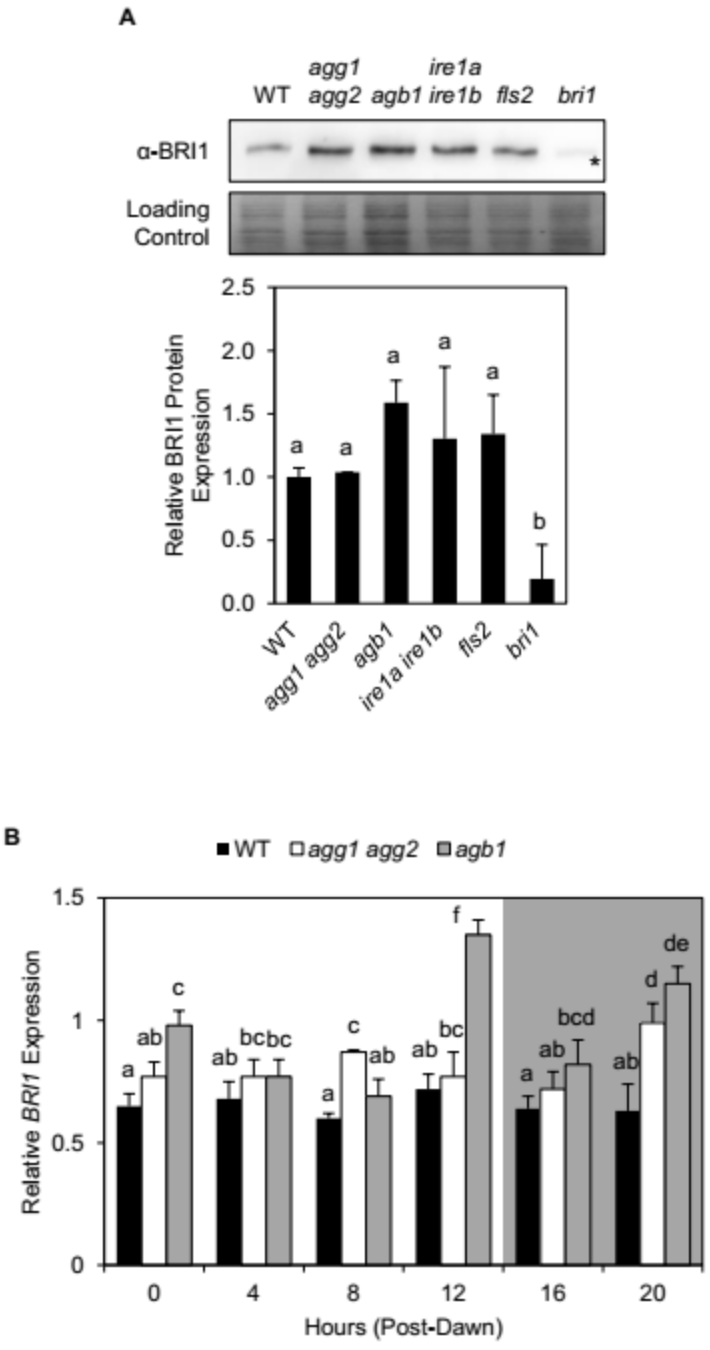

Supplementary Figure S2.

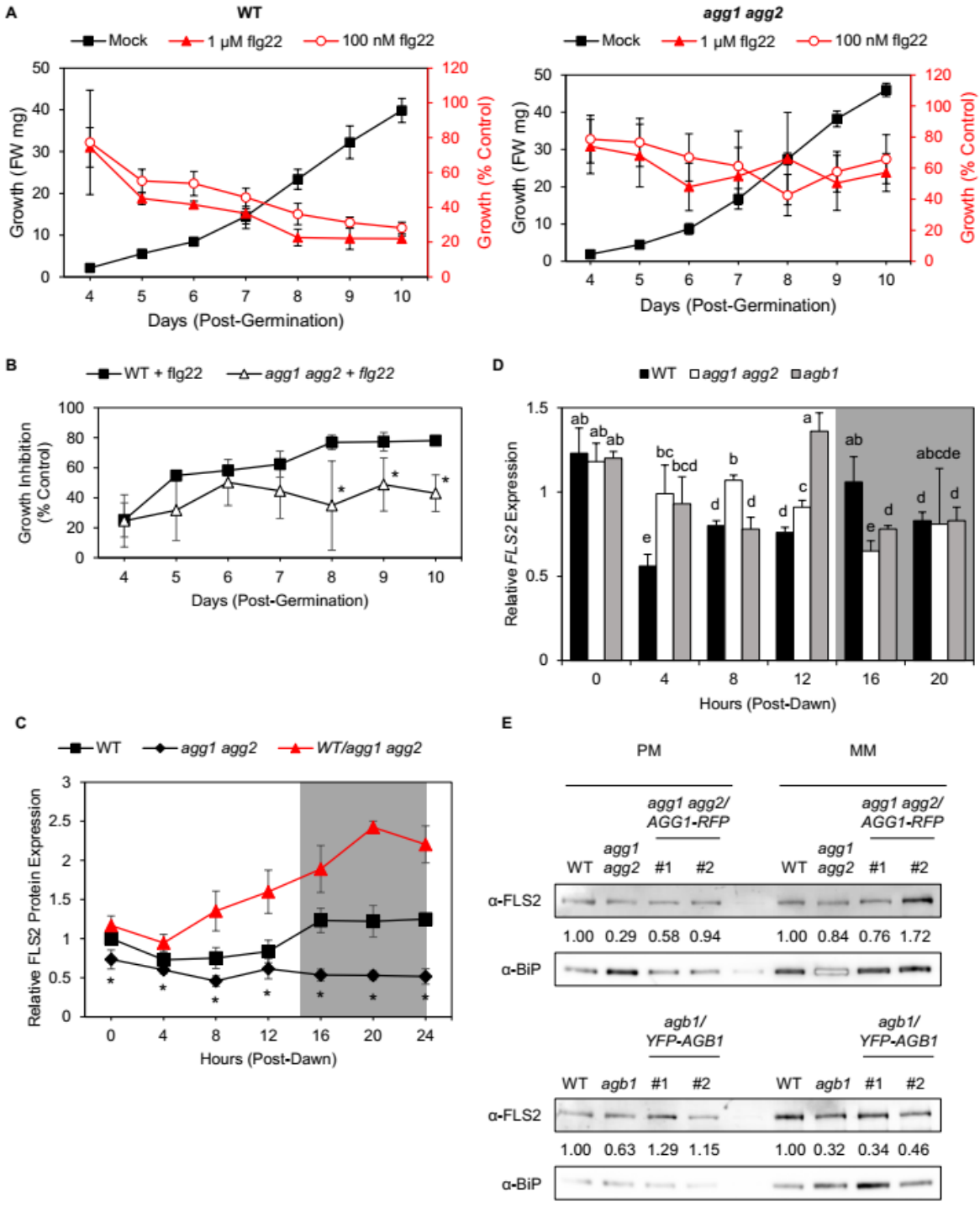

Supplementary FigureS3.

912

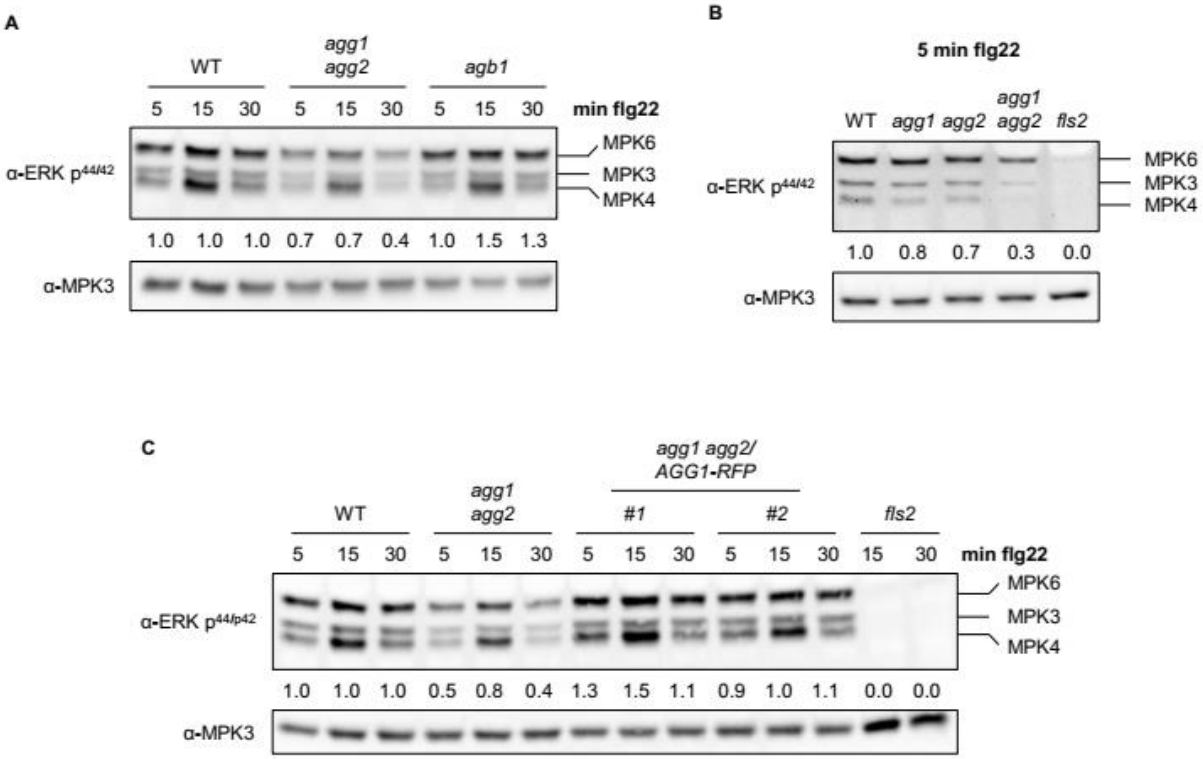

Supplementary Figure S4.

913

914

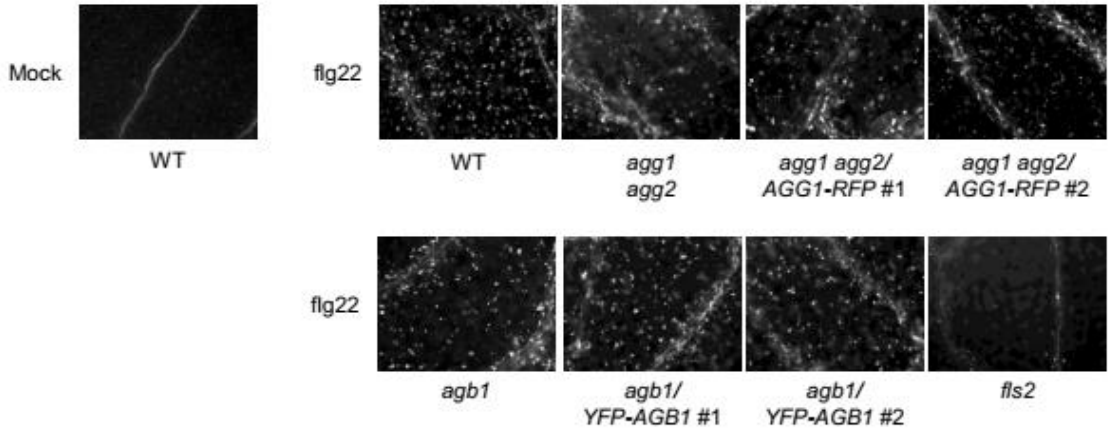

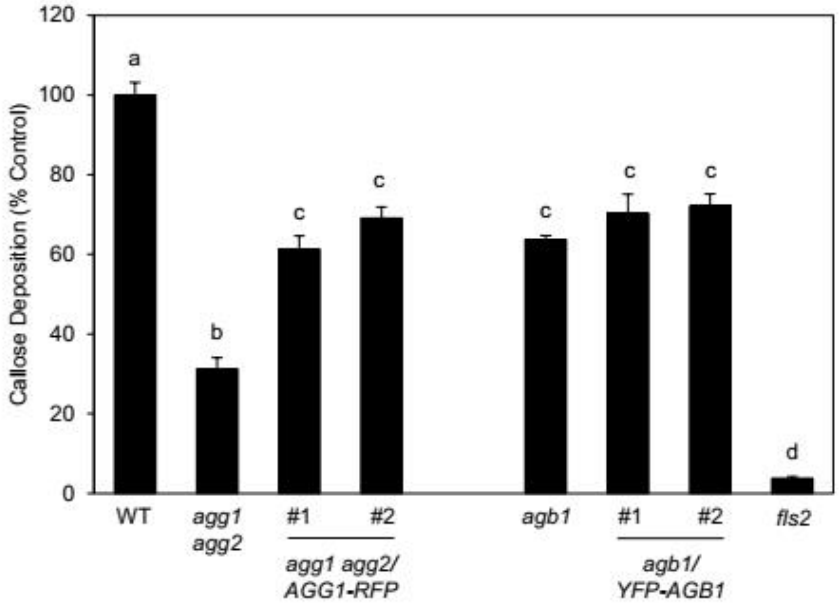

Supplementary Figure S5.

915

916

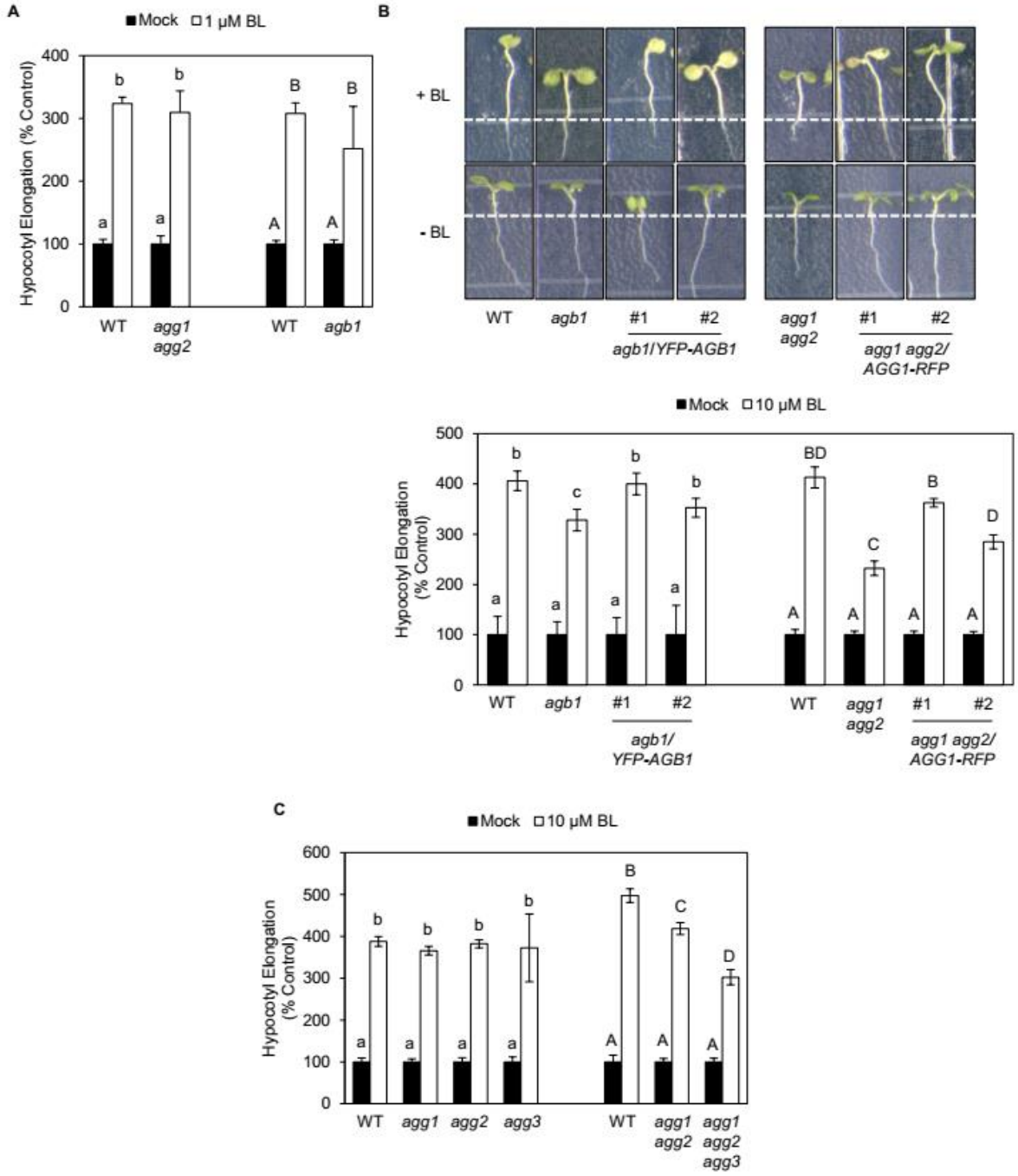

Supplementary Figure S6.

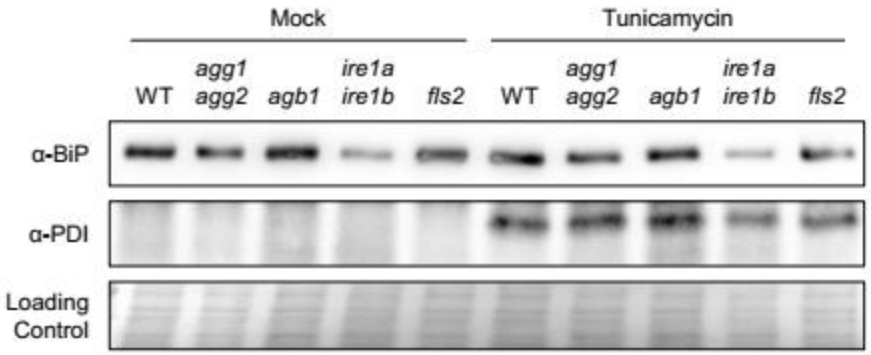

Supplementary Figure S7.

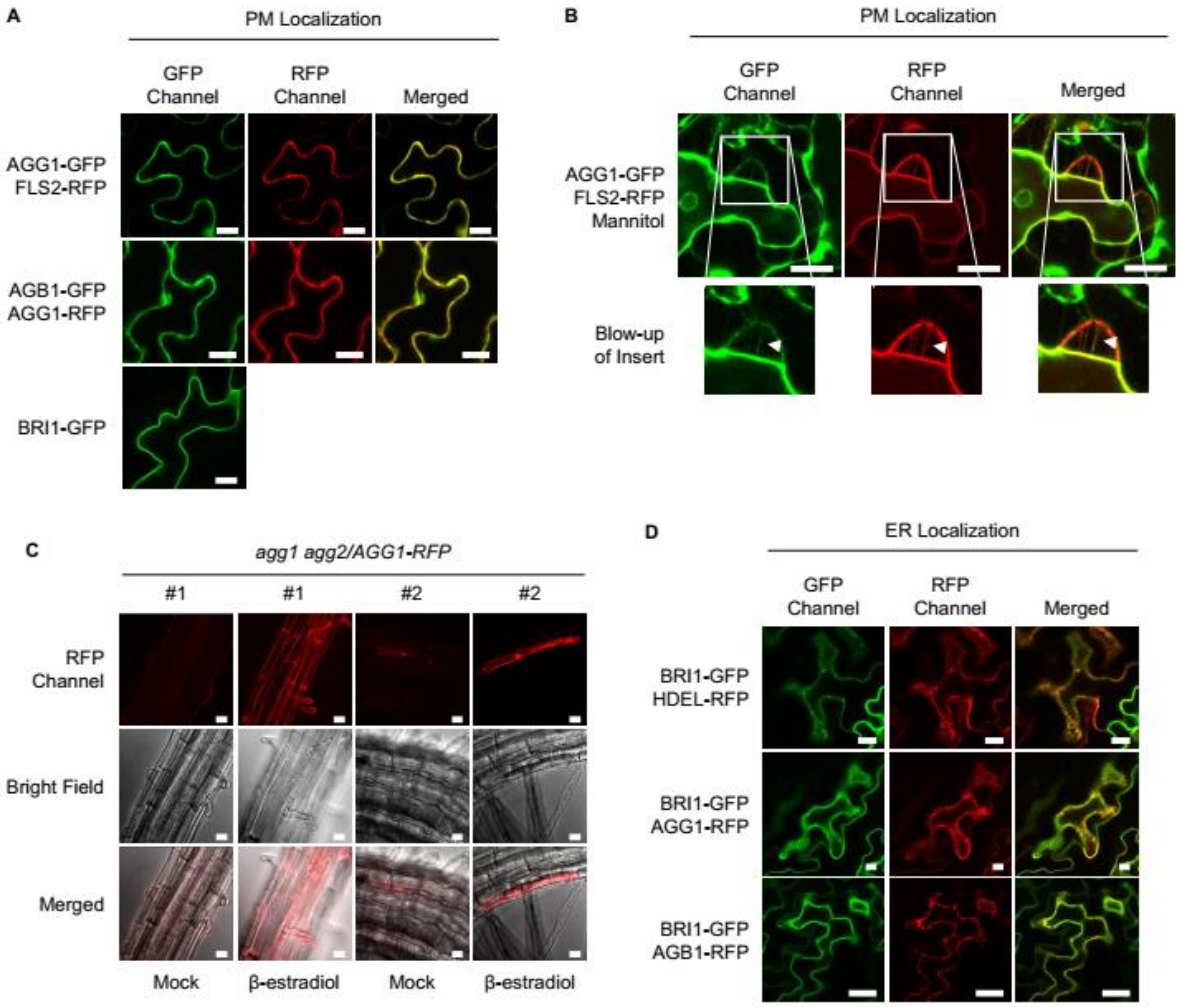

Supplementary Figure S8.

921

922

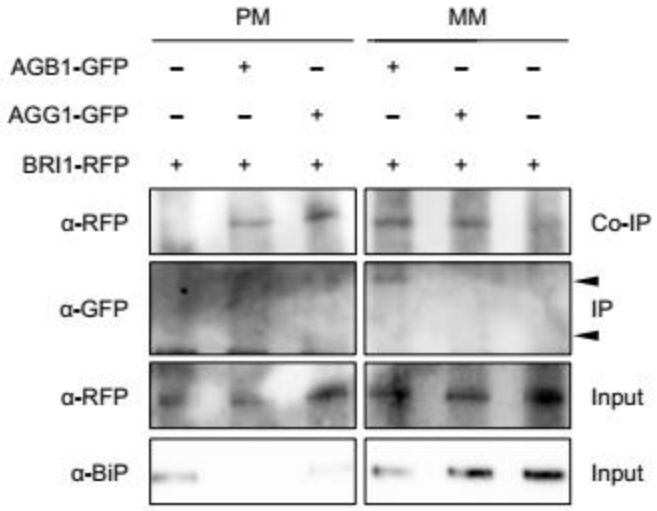

Supplementary Figure S9.

923

924

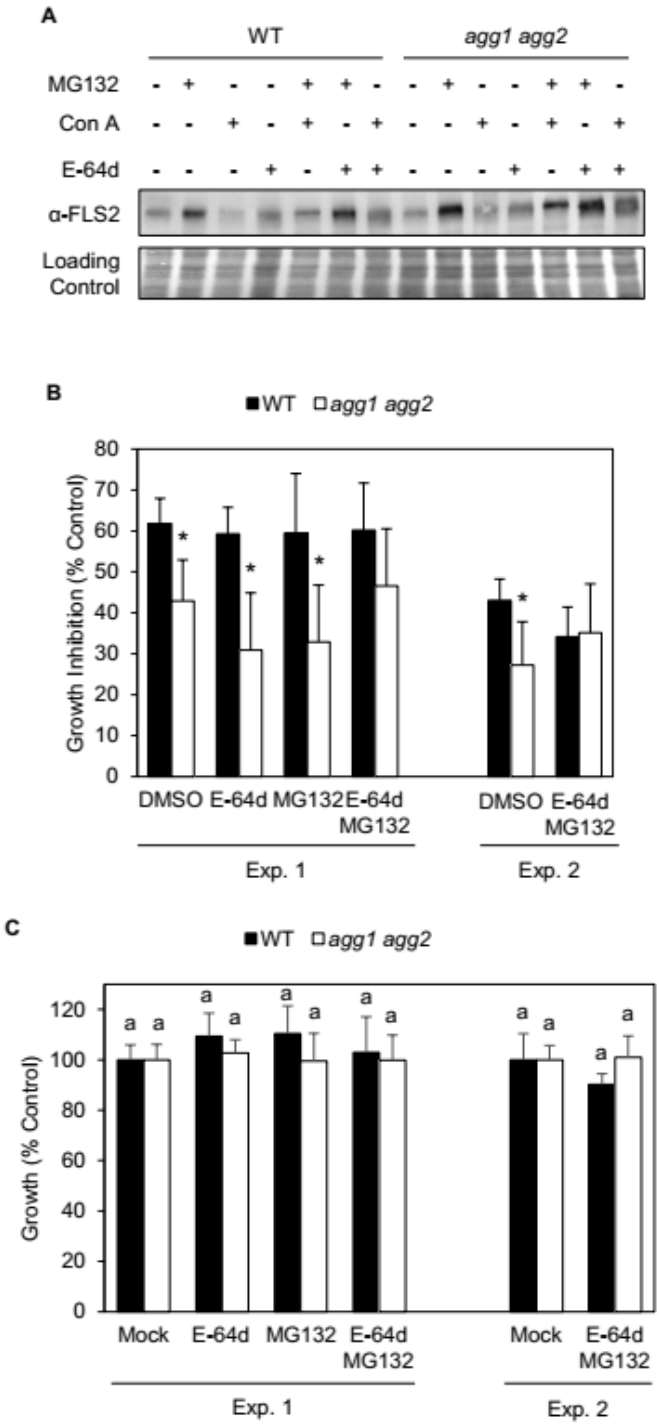

Supplementary Figure S10.

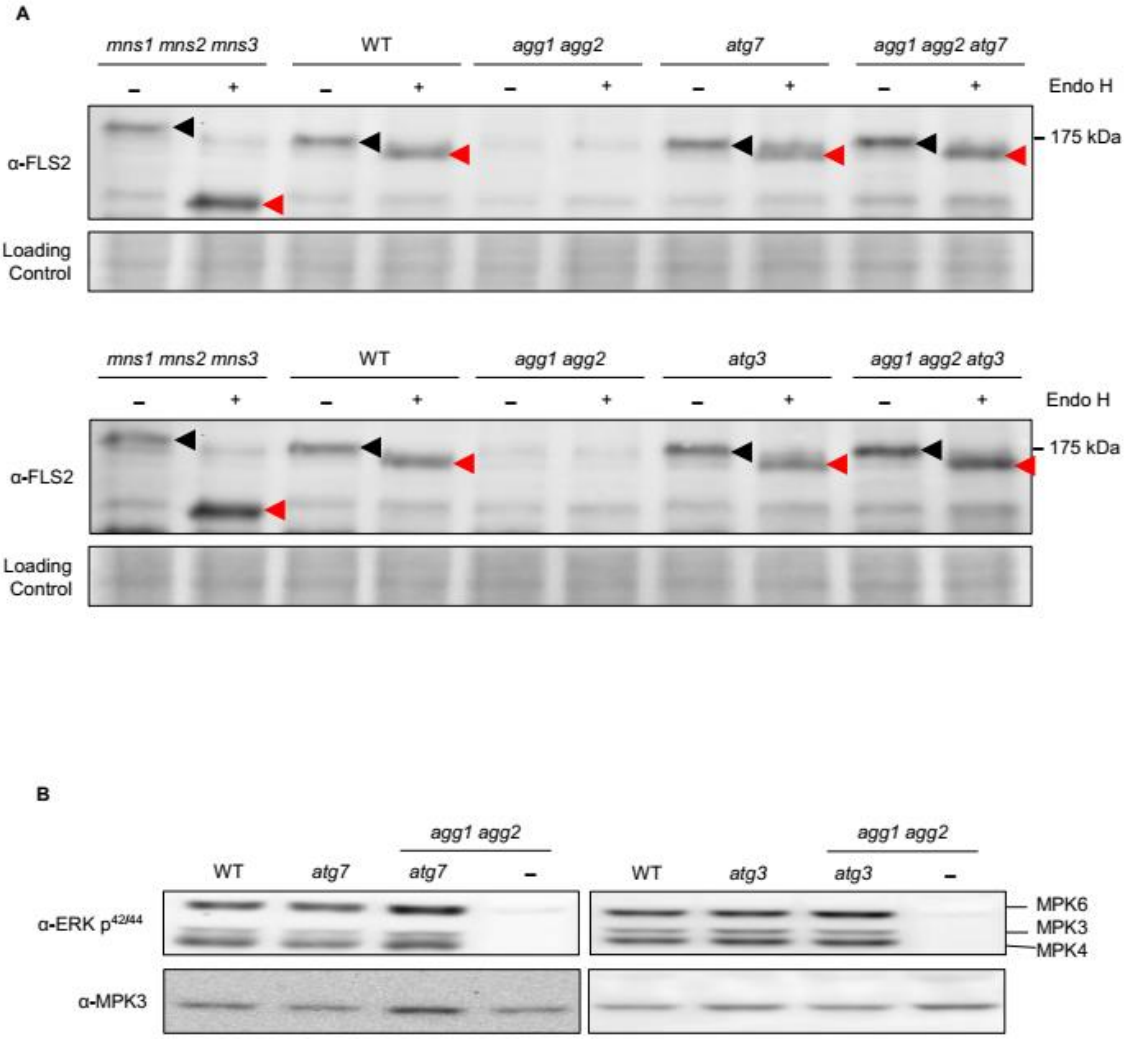

Supplementary Figure S11.

926

927

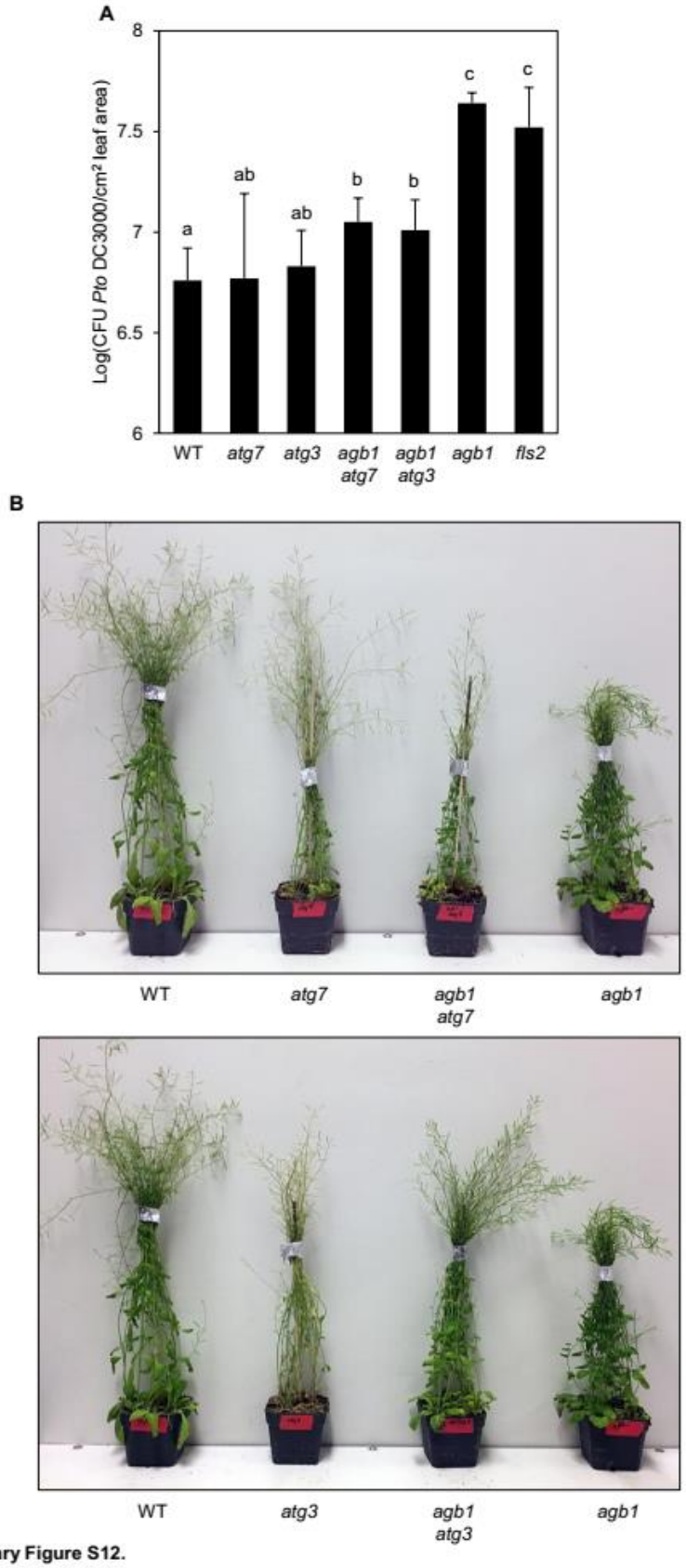

Supplementary Figure S12.

928

929

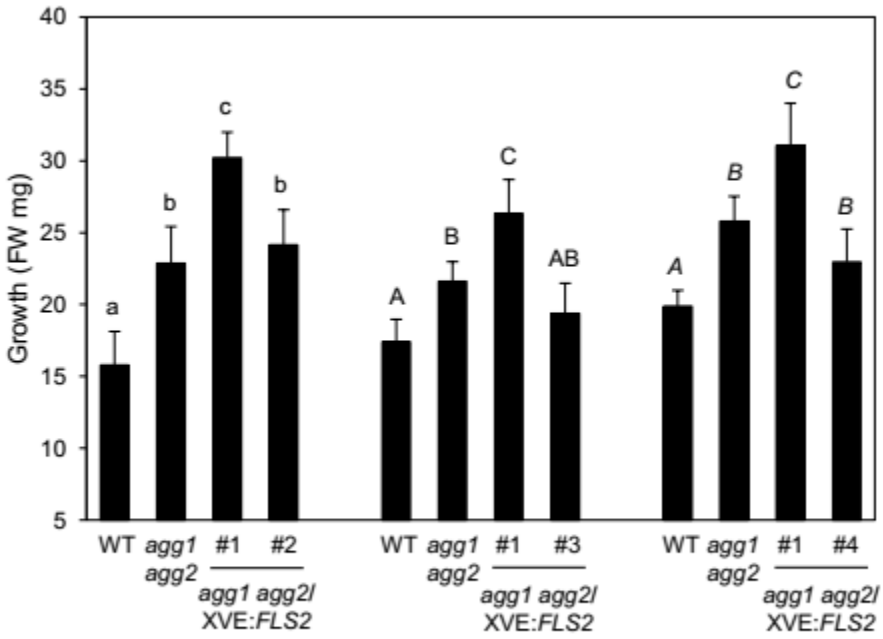

Supplementary Figure S13.

930

931

932 **Table S14. qPCR primer sequences and efficiencies.**

Gene		Primer Sequence	Pimer Efficiency (%)	Efficiency Temp. (°C)
AGB1	Forward	5'-CTGATGTACTAAGCGTCTC-3'	97.6	53
	Reverse	5'-ATGAAAGGTACGCACTGCT-3'		
AGG1	Forward	5'-GTTGAACAGGAAGTCGCTT-3'	93.5	53
	Reverse	5'-TCTCGATGACAGATAGCAG-3'		
AGG2	Forward	5'-CAAGAAGCTCGATTCTTAGA-3'	91.9	53
	Reverse	5'-GTTTGCTGTCAACACTGTC-3'		
BRI1	Forward	5'-AACAAAAGGAGACGTTTATAGT-3'	90	55
	Reverse	5'-CAGTTTTGCGTGCTGTTTCA-3'		
CYP81F2	Forward	5'-CTCATGCTCAGTATGATGC-3'	86.2	53
	Reverse	5'-CTCCAATCTTCTCGTCTATC-3'		
CYP82C2	Forward	5'-CAAGCATGTCCGTGTTTCTG-3'	91.6	53
	Reverse	5'-GCATCTTCAGGGGATAACGA-3'		
EIF4A	Forward	5'-TCTGCACCAGAAGGCACA-3'	100	55
	Reverse	5'-TCATAGGATGTGAAGAACTC-3'		
FLS2	Forward	5'-ATACTCCTTGACAGTGACC-3'	100	55
	Reverse	5'-AACTCTGGAGCTAAGTATCC-3'		
FRK1	Forward	5'-GCAAGGACTAGAGTATCTTC-3'	96.5	53
	Reverse	5'-ATCTTCGCTTGGAGCTTCT-3'		
IRE1A	Forward	5'-ACGATAGCATCCGTGACTT-3'	84.6	55
	Reverse	5'-TGTTCCGACAAGTTCCTGA-3'		
IRE1B	Forward	5'-AATGAGATAGTGGATGCTTC-3'	98.5	53
	Reverse	5'-CCAAGAGAAACACAGATGTA-3'		

933

934